Proton magnetic resonance spectroscopy in the brain: Report of AAPM MR Task Group #9

Dick J. Drost[a)]
Nuclear Medicine and MRI Department, St. Joseph's Health Centre, London, Ontario N6A 4L6, Canada

William R. Riddle
Department of Radiology and Radiological Sciences, Vanderbilt University Medical Center, Nashville, Tennessee 37232-2675

Geoffrey D. Clarke
Department of Radiology, Division of Radiological Sciences, University of Texas Health Sciences Center, San Antonio, Texas 78284

(Received 28 January 2002; accepted for publication 14 June 2002; published 27 August 2002)

AAPM Magnetic Resonance Task Group #9 on proton magnetic resonance spectroscopy (MRS) in the brain was formed to provide a reference document for acquiring and processing proton (^{1}H) MRS acquired from brain tissue. MRS is becoming a common adjunct to magnetic resonance imaging (MRI), especially for the differential diagnosis of tumors in the brain. Even though MR imaging is an offshoot of MR spectroscopy, clinical medical physicists familiar with MRI may not be familiar with many of the common practical issues regarding MRS. Numerous research laboratories perform *in vivo* MRS on other magnetic nuclei, such as ^{31}P, ^{13}C, and ^{19}F. However, most commercial MR scanners are generally only capable of spectroscopy using the signals from protons. Therefore this paper is of limited scope, giving an overview of technical issues that are important to clinical proton MRS, discussing some common clinical MRS problems, and suggesting how they might be resolved. Some fundamental issues covered in this paper are common to many forms of magnetic resonance spectroscopy and are written as an introduction for the reader to these methods. These topics include shimming, eddy currents, spatial localization, solvent saturation, and post-processing methods. The document also provides an extensive review of the literature to guide the practicing medical physicist to resources that may be useful for dealing with issues not covered in the current article. © *2002 American Association of Physicists in Medicine.*
[DOI: 10.1118/1.1501822]

Key words: magnetic resonance spectroscopy, medical brain imaging, brain metabolism

TABLE OF CONTENTS

I. INTRODUCTION

Proton magnetic resonance spectroscopy (MRS) is provided as an option by most manufacturers and is becoming more common in clinical practice, particularly for neurological applications. Although MRS can be performed on nuclei such as ^{31}P and ^{13}C, proton (^{1}H) MRS requires only a software package plus a test phantom, making it the easiest and least expensive spectroscopy upgrade for the MRI system. Non-proton spectroscopy requires radio frequency (RF) coils tuned to the Larmor frequency of other nuclei plus matching preamplifiers, hybrids, and a broad-band power amplifier. Proton MRS software packages automate acquisition sequences and post-processing for metabolite quantification.[1] However, the efficient implementation of MRS acquisition protocols is something that is beyond the expectations for most MR technologists. Therefore, MR physicists are often called in to perform MRS procedures to evaluate whether problems with proton MRS are due to equipment malfunctions, software problems, or operator errors. We give a brief overview of clinical proton MRS, discuss some common clinical MRS problems, and suggest how they might be resolved.

A. Larmor equation

In magnetic resonance, nuclei resonate at a frequency (f) given by the Larmor equation

$$f=\gamma B_0, \tag{1}$$

where B_0 is the strength of the external magnetic field and γ is the nucleus' gyromagnetic ratio. For protons, γ is equal to 42.58 MHz/Tesla. If all the proton nuclei in a mixture of molecules had the same Larmor frequency, magnetic resonance spectra would be limited to a single peak. However, the magnetic B_0 field ''seen'' by a nucleus is shielded by the covalent electron structure surrounding the nucleus. Therefore, nuclei with different chemical neighbors will have slightly different resonance frequencies (f) given by

$$f=\gamma B_0(1-\sigma_{cs}), \tag{2}$$

where σ_{cs} is a screening constant ($|\sigma_{cs}|\ll 1$). This small change in the resonance frequency is the basis for magnetic resonance spectroscopy. Note that both the overall molecular structure and the proton(s) position within the molecule will determine σ_{cs} or f.

B. Magnetic resonance signal

In spectroscopy, the strength of the MR signal is proportional to the number of protons at that frequency. While spectroscopy can be described in the time domain, MRS data are usually displayed in the frequency domain. In the frequency domain, the area under a specific peak is proportional to the number of protons precessing at that frequency. The frequency axis itself is reversed from ''normal'' for historical precedent. Before the introduction of the Fast Fourier Transform[2] (FFT) in 1965, almost all spectrometers employed continuous-wave irradiation, which swept either the applied magnetic field (an electromagnet) or the transmitter frequency. The abscissa for spectra went from low field to high field, which means that protons precessing at the highest frequencies would be recorded first (left-hand side). Now almost all spectrometers use the FFT, but spectra are still displayed historically with the abscissa displaying decreasing frequency from left to right.

C. Parts per million (ppm) scale

Although one could use a frequency axis to display spectra, two problems arise with this type of display. One, the axis is proportional to B_0 [Eq. (2)] which means that peak locations on an axis will depend on the B_0 field used for the measurement. Second, there is no natural material to represent zero frequency. To overcome these problem, NMR chemists mix the substance to be measured with a reference, then express the frequency difference between the substance and the reference as a dimensionless quality, δ_{cs} (in parts per million), given by

$$\delta_{cs}=\frac{(f_s-f_{ref})}{f_{ref}\times 10^{-6}}, \tag{3}$$

where f_s is the frequency of the substance (laboratory frame) and f_{ref} is the frequency of the reference (laboratory frame). The reference used in proton spectroscopy is TMS {tetramethyl-silane [$(CH_3)_4Si$]}, and its single peak is assigned a chemical shift of 0.0 ppm. Another reference used is DSS (2,2-dimethyl-2-silapentane-5-sulfonate), and its major peak is at 0.0 ppm. Figure 1 displays the ppm axis and demonstrates that the horizontal peak spacing remains constant in ppm when collecting data at 1.5 T and at 3.0 T.

Since TMS and DSS are toxic, they are not used in *in vivo* spectroscopy. When spectra are acquired without TMS or DSS, another equation for δ_{cs} is as follows:

$$\delta_{cs}=\frac{f_s}{f_{transmitter}\times 10^{-6}}+\text{offset}, \tag{4}$$

where f_s is the frequency of the sample (rotating frame), $f_{transmitter}$ is the frequency of the transmitter (laboratory frame), and offset is a constant that references the ppm scale to an *in vivo* standard, which for ^{1}H brain spectroscopy, is usually the CH_3 peak of N-acetyl aspartate (NAA) with a chemical shift value of 2.01 ppm. Knowing the chemical shift of a peak, the value for offset can be determined by using the measured frequency (f_s) of the peak, the chemical shift of the peak (δ_{cs}), and the transmitter frequency. Once determined, this offset can be used to change all frequencies in a spectrum from Hz to ppm. For example with $\delta_{cs}=2.01$ ppm, $f_s=-171.8$ Hz, and $f_{transmitter}=63\,863\,375$ Hz, the offset is equal to 4.700 ppm. In this example the transmitter frequency, $f_{transmitter}$, was centered on water. Note that the resonance frequency of water is dependent on temperature, with frequency increasing as temperature decreases ($\Delta\text{ppm}/\Delta\,^{\circ}\text{C}=-0.01$ ppm/°C).[3] At 37 °C, δ_{cs} of water is 4.70 ppm; at 20 °C, δ_{cs} of water is 4.87 ppm. Therefore water is not a good internal standard for the ppm scale.

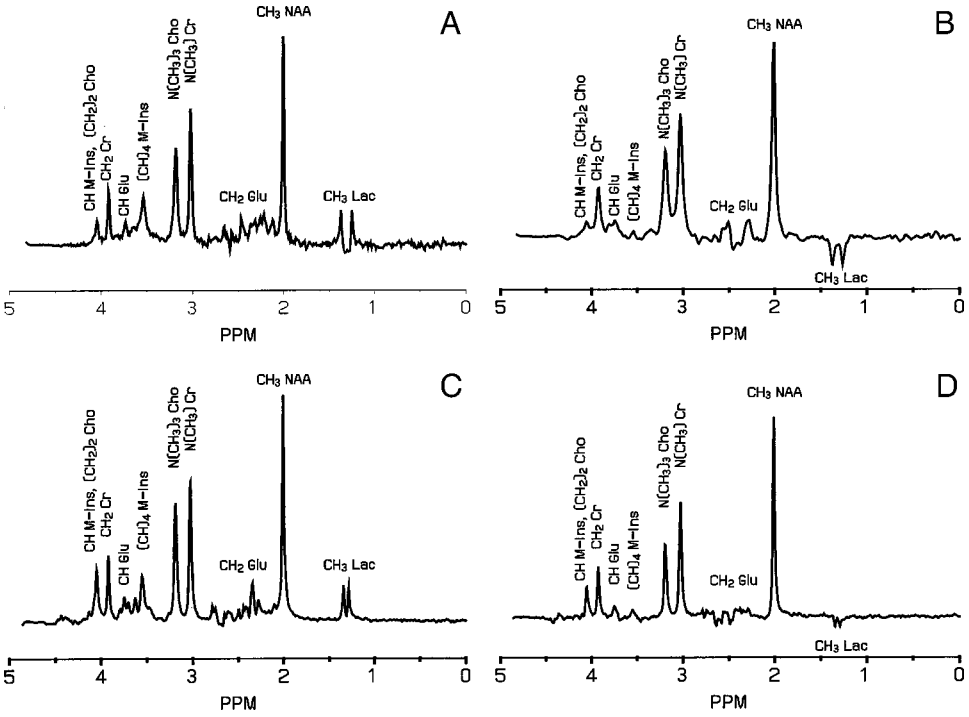

FIG. 1. Spectra from a test phantom containing 12.5 mM NAA, 10.0 mM Cr, 3.0 mM Cho, 12.5 mM Glu, 7.5 mM M-Ins, and 5.0 mM Lac at 1.5 T [panels (A) and (B)] and 3 T [panels (C) and (D)]. All were acquired with a PRESS sequence, TR = 1500 ms, 32 averages, and voxel size = 8 cm^3. Panels (A) and (C) have TE = 36 ms and panels (B) and (D) have TE = 144 ms.

D. *J* coupling

Another feature of spectra is peak splitting or multiplets, as shown by lactate (CH_3-Lac) in Fig. 1. Multiplets are caused by *J* coupling (spin–spin) which is explained in Refs. 4–7. With *J* coupling, the nuclear magnetic energy levels are split by quantum interactions, via covalent bond electrons, with other nuclei whose magnetic moments may be parallel or antiparallel to the main magnetic field. *J* coupling can be homonuclear (e.g., $^1H-^1H$) or heteronuclear (e.g., $^1H-^{13}C$).

The following is a more intuitive, classical explanation of *J* coupling. Suppose nucleus *A* is coupled to nucleus *X* and nucleus *X* has an equal probability of being in a parallel or an antiparallel spin state. Nucleus *A* will be split into two equal peaks. The peak of nucleus *A* that is coupled to nucleus *X* parallel to the main field will have higher frequency; the peak of nucleus *A* that is coupled to nucleus *X* antiparallel to the main field will have lower frequency. For lactate, the CH_3 nucleus at 1.31 ppm is coupled to the CH nucleus at 4.10 ppm, and the CH_3 nucleus is split into two equal peaks (doublet) separated by 6.93 Hz.[4]

Peak splitting from *J* coupling has the same absolute value in Hz, regardless of the main magnetic field strength. References 4 and 8 and Table I have a list of *J* coupling constants for other metabolites. *J* coupling also causes phase evolutions that cause peak and baseline distortions that vary with echo time (TE)[5–7] and field strength, as shown by glutamate and lactate in Fig. 1. *J* coupling explains the well-known observation that the lactate doublet has negative peaks (180° out of phase) at TE≈140 ms for a PRESS sequence [Fig. 1(B)]. Less known is that *J* coupling also causes overlapping multiplet peaks within individual metabolites and between metabolites to cancel each other due to dephasing at later echo times under typical *in vivo* field homogeneities. For this reason, metabolites such as glutamine (Gln), glutamate (Glu), and γ-aminobutyric acid (GABA) cannot be measured using long echo times (TE > 50 ms) with *in vivo* proton spectroscopy.[8] (However Ref. 89 uses a CPMG type sequence to overcome this problem.) On the plus side, spectral editing, a spectroscopy technique that uses *J* coupling to eliminate overlapping peaks, can be used to quantify concentrations of an underlying peak allowing the *in vivo* measurement of metabolites such as GABA.[9–11]

E. Brain metabolites

Metabolites containing protons that can be measured in the brain at 1.5 Tesla include N-acetyl aspartate (NAA), considered to be present only in neurons and dendrites; N-acetylaspartylglutamate (NAAG), suggested to be involved in excitatory neurotransmission; creatine/phosphocreatine (Cr), a reservoir for high energy phosphate for generation of adenosine triphosphate (ATP); choline/phosphocholine/glycerophosphorylcholine (Cho), associated with glial cell membrane integrity; GABA, glutamate (Glu), and glutamine (Gln), important in neurotransmission, but very difficult to quantify *in vivo* due to multiplets and *J* coupling effects; myo-inositol (M-Ins), important in cell growth and possibly a glial cell marker; and sometimes lactate (Lac), indicative of anaerobic metabolism. Although NAA is considered a neuronal marker, changes in NAA from normal may reflect reversible changes in neuronal metabolism rather than irreversible changes in neuronal density. Ross *et al.* have a good discussion on neurometabolism and the clinical application of *in vivo* ^1H MRS.[12,13] Table I lists some additional ^1H metabolites which can be detected using short (e.g., TE = 20) single voxel spectroscopy under optimum conditions.[4,14] In addition to these metabolites, *in vivo*

TABLE I. Metabolites observed with brain MRS (Ref. 4). Multiplicity definitions are *s*, singlet; *d*, doublet; *dd*, doublet-of-doublets; *t*, triplet; *q*, quartet; *m*, multiplet. Note that T1 and T2 values for metabolites (Ref. 85) are offered for comparison only and may vary somewhat with B_0 magnetic field strength in various tissues.

Metabolite	δ_{cs} (ppm)	Conc. (mM/kg_{ww})	Number of protons	Multiplicity	J (Hz)	T1 (ms)	T2 (ms)
CH_3 lipid	0.94		3				
CH_3 lactate	1.31	0.4	3	*d*	6.933		
CH_2 lipid	1.33		2				
CH lipid	1.5		1				
CH_3 NAA	2.01	7.9–16.6	3	*s*	None	1368	376
CH_3 NAAG	2.04	0.6–2.7	3	*s*	None		
CH_2 Glu	2.04	6.0–12.5	2	*m*	4.651		
CH_2 Glu	2.12	6.0–12.5	2	*m*	−14.85		
CH_2 Glu	2.34	6.0–12.5	2	*m*	8.406		
CH_2 Glu	2.35	6.0–12.5	2	*m*	6.875		
CH_2 NAA	2.49	7.9–16.6	2	*dd*	−15.59		
CH_2 NAA	2.67	7.9–16.6	2	*dd*	9.821		
$N(CH_3)$ Cr	3.03	5.1–10.6	3	*s*	None	1424	217
$N(CH_3)_3$ Cho	3.19	1.5–2.5	9	*s*	None	1369	346
$(CH)_4$ M-Ins	3.52	3.8–8.1	4	*dd*	3.006	1124	162
CH Glu	3.74	6.0–12.5	1	*dd*	7.331		
CH_2 Cr	3.91	5.1–10.6	2	*s*	None		
$(CH_2)_2$ Cho	4.05	1.5–2.5	4	*m*	3.14		
CH M-Ins	4.05	3.8–8.1	1	*t*	9.998		
CH lactate	4.10	0.4	1	*q*	6.933		
H_2 water (37°)	4.70	36 M	2	*s*	None	380–1470	60–130

brain proton MR spectra may also contain peaks due to water, lipids, and macromolecules.[15,16] The methods used to deal with the signals from these last three categories of chemicals, when they are unwanted, are discussed below.

F. Magnetic field homogeneity

Spectral resolution is determined primarily by three factors. First, the transverse relaxation time (T_2) of the metabolite is inversely proportional to the ideal peak width. Second, the B_0 separation between peaks (in Hz) increases linearly with magnetic field strength. Third, the local magnetic field inhomogeneities widen and distort the spectral lines from their ideal Lorentzian forms. Maximum homogeneity is accomplished by adjusting DC currents in the gradient coils and room temperature shim coils. The name for this process is ''shimming,'' which is a historical term that is derived from a time when magnetic resonance researchers were working on resistive pole–gap magnets and adjusted the magnetic field by placing thin brass shim stock between the magnet and pole faces to make them parallel. Shimming is discussed in some detail in Sec. V.

II. TEST PHANTOM

The MR system's manufacturer will supply a test phantom, usually an 18 to 20 cm diameter sphere containing ^{1}H metabolites. Figure 1 shows spectra from a test phantom containing 12.5 mM NAA, 10.0 mM Cr, 3.0 mM Cho, 12.5 mM Glu, 7.5 mM M-Ins, and 5.0 mM Lac with TE=36 ms and TE=144 ms. These concentrations emulate *in vivo* brain concentrations. Because test phantoms lack many *in vivo* metabolites, lipids, macromolecules, and susceptibility problems, they lead to well-resolved spectra with flat baselines, facilitating the detection of MRS acquisition or post-processing problems. A good MRS phantom is also required for an effective MRS quality control (QC) program.

III. SPECTROSCOPIC SEQUENCES

The most common *in vivo* ^{1}H spectroscopy acquisition techniques are STimulated Echo Acquisition Mode (STEAM)[17] and Point-RESolved Spectroscopy (PRESS).[18] Both of these sequences use three slice-selective radio-frequency pulses with orthogonal magnetic field gradients where the intersection of the slices defines the volume of interest (VOI). The three RF pulses produce FIDs, multiple spin echoes (SE), and a stimulated echo (STE).[5,19] Four time intervals $(\tau_1, \tau_2, \tau_3, \tau_4)$ associated with the RF pulses are defined as follows: τ_1 is the time between the first and second RF pulses, $\tau_2+\tau_3$ is the time between the second and third RF pulses, and τ_4 is some time period after the third RF pulse. The FID of the first RF pulse refocused by the second RF pulse [SE(1,2)] occurs at $2\tau_1$. If $2(\tau_2+\tau_3)>2\tau_1$, the echo SE(1,2) is refocused by the third RF pulse to produce the spin echo, SE(2,1), at $2(\tau_2+\tau_3)$. The FID from the second RF pulse refocused by the third RF pulse [SE(2,3)] occurs at $\tau_1+2(\tau_2+\tau_3)$. The FID from the first RF pulse refocused by the third RF pulse [SE(1,3)] occurs at $2(\tau_1+\tau_2+\tau_3)$. The stimulated echo occurs at $2\tau_1+\tau_2+\tau_3$. Note that all times are from the center of the first selective RF pulse. Also see Fig. 2.29 in Ref. 5.

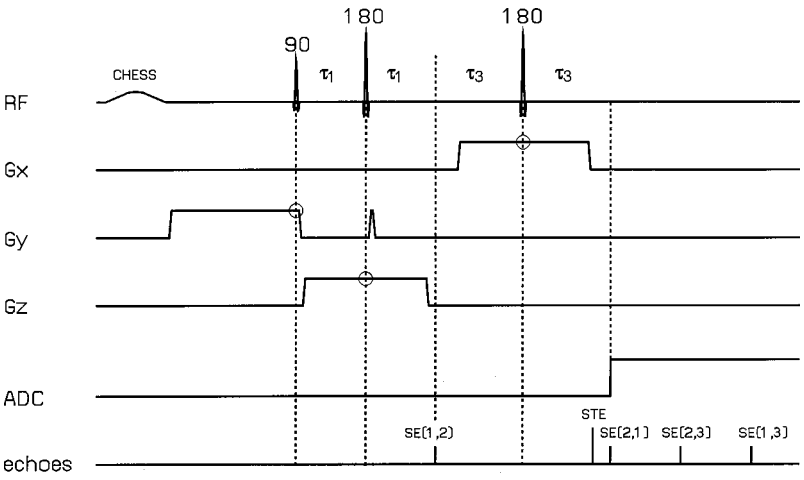

FIG. 2. Timing diagram for a PRESS sequence with one CHESS pulse for water suppression. The circles in the timing diagram demark the duration of the slice selection gradients necessary for defining the VOI. Although the gradient areas outside the circles are used for spoiling, more spoiling can be added with equal area gradients on each side of the 180 degree pulses on the other axis (Ref. 22). Additional water spoiling gradients can be added between the CHESS and the first RF pulse.

A. Point RESolved spectroscopy (PRESS)

A PRESS sequence has three slice-selective RF pulses with the form of $90°$-τ_1-$180°$-$(\tau_2+\tau_3)$-$180°$-τ_4-SE(2,1). Figure 2 shows a PRESS timing diagram [with one CHEmical-Shift-Selective (CHESS) pulse for water suppression[20]]. With a PRESS sequence, $\tau_1=\tau_2$ and $\tau_3=\tau_4$. The TE of the SE(2,1) in this PRESS sequence is equal to $\tau_1+\tau_2+\tau_3+\tau_4$. The circles in the timing diagram show the slice selection gradients necessary for defining the VOI. The other gradients are used to dephase the spins from the CHESS pulse and to suppress all the NMR signals except SE(1,2) and SE(2,1).

B. Stimulated echo acquisition mode (STEAM)

A STEAM sequence has three slice-selective RF pulses with the form of $90°$-τ_1-$90°$-$(\tau_2+\tau_3)$-$90°$-τ_4-STE. Figure 3 shows a STEAM timing diagram with one CHESS pulse. For the STEAM sequence, τ_1 is equal to τ_4, $\tau_1+\tau_4$ is the echo time, and $\tau_2+\tau_3$ is called the mixing time (TM). An important feature of STEAM is that only half of the transverse magnetization prepared by the first $90°$ pulse is transformed into longitudinal magnetization by the second $90°$ pulse, decreasing signal-to-noise (S/N) by a factor of 2. During the TM period, longitudinal magnetization decays with T1 rather than T2. The third RF pulse transforms the longitudinal magnetization stored by the second RF pulse back into the transverse plane to form the stimulated echo. The circles in the timing diagram show the slice selection gradients necessary for defining the VOI. The other gradients are used to dephase the spins from the CHESS pulse and to suppress all the spin echoes, leaving only the stimulated echo. In practice, both PRESS and STEAM use several crusher gradients after each RF pulse to dephase unwanted signals from echoes and FIDs.[21–23] Although more crusher gradients can be added, this increases the probability of eddy current artifacts in the spectrum. Typical clinical *in vivo* ^{1}H-MRS acquisitions have TEs of 20 ms with STEAM and 30 ms or 135 ms with PRESS; TRs greater than or equal to 1.5 s; and data acquisition times of 1 s. Research MRS groups have reduced TE from 1 to 6 ms with STEAM and to 13 ms with PRESS.[21,24,25]

C. PRESS and STEAM spectra

Examples of PRESS and STEAM spectra are shown in Fig. 4. Both spectra were acquired at 1.5 T with the same receiver gain settings, an 8 ml VOI, TE=288 ms, TR=1500 ms, and 32 signal averages. The measured noise for the PRESS spectrum and the STEAM spectrum was the same. A comparison of the unsuppressed water and water-suppressed NAA peaks is given in Table II. In this table, signal is pro-

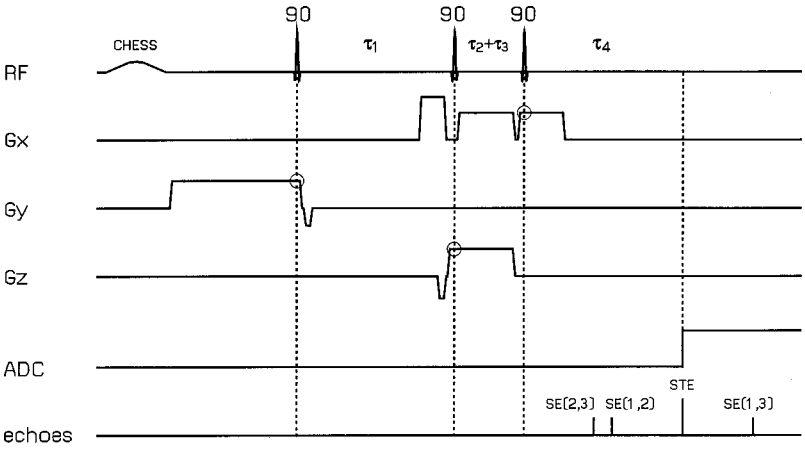

FIG. 3. Timing diagram for a STEAM sequence with one CHESS pulse for water suppression. The circles in the timing diagram demark the duration of the slice selection gradients necessary for defining the VOI. Although the gradient areas outside the circles are used for spoiling, more spoiling can be added by turning on the G_y gradient during the TM period and placing equal gradient areas in the τ_1 and τ_4 intervals. Additional water spoiling gradients can be added between the CHESS and the first RF pulse.

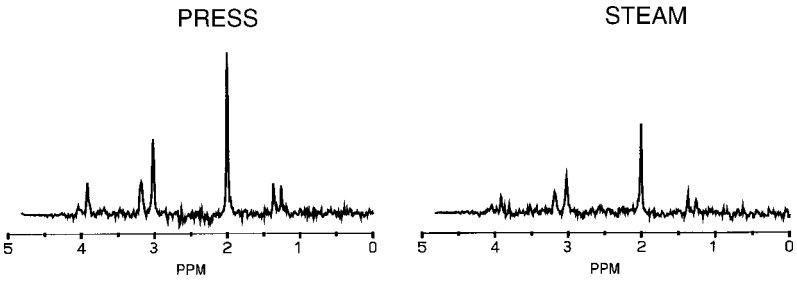

FIG. 4. PRESS and STEAM spectra from a test phantom (same as Fig. 1) acquired with the same receiver gain, 8 ml VOI, TE=288 ms, TR=1500 ms, and 32 averages. Theory predicts that the PRESS acquisition has twice the S/N as the STEAM acquisition. Also note the difference in J coupling effects between PRESS and STEAM in the 4 ppm and 2.5 ppm regions.

portional to peak height and peak area is proportional to (peak height×FWHM). The product of S/N and FWHM with STEAM is 0.6 that found with PRESS (for the same TE), although theoretically it should be 0.5. The main reason for the discrepancy is the poor VOI profiles due to the 180° RF slice selective pulses compared to 90° RF pulses. Poorer slice profiles also lead to more out-of-volume contamination that results in larger lipid peaks *in vivo* and baseline distortion.[22] There are also other differences between STEAM and PRESS.[26] Because STEAM uses only 90° RF pulses with a TM period, the TE can be shorter than with a PRESS sequence, which reduces signal decay and distortion due to J coupling. Large and lengthy crusher gradients can be applied during the TM interval to dephase unwanted signals which will reduce out of volume contamination.[22] The specific absorption ratio (SAR) with PRESS is about twice that with STEAM. Finally, the effects of J coupling can change whether STEAM or PRESS is used, although the effects depend more on the TM, TE, and actual flip angles chosen.[6,7,14,27] There is an additional complication in that the chemical shift that occurs with RF selective slices means that a particular metabolite such as lactate has coupled nuclei which are excited by one RF pulse, but not necessarily both the remaining two selective RF pulses. This can lead to signal cancellation within the voxel, which depends on both the type of sequence and the bandwidth of the RF pulses.[28]

D. Chemical shift imaging

STEAM or PRESS can either be used to acquire data from a single voxel or from multiple voxels using chemical shift imaging (CSI).[5,18,29–36] Phase encoding gradients are used in CSI spectroscopy to encode spatial information analogous to imaging. The selected CSI volume to be phase-encoded will be larger than a single volume acquisition. A typical CSI acquisition will select a 10 cm×10 cm×2 cm volume using three RF selective pulses with a STEAM or PRESS sequence and phase encode this CSI volume with 16×16 phase encode steps on a 16×16 cm FOV. This results in 100 voxels of data with a nominal voxel size of 1×1×2 cm^3. However, to minimize the sinc point spread function of each reconstructed voxel (Gibb's ringing in imaging), a k-space filter (typically 50% Hamming) is applied before reconstruction, which effectively increases the voxel size in this example to 1.5×1.5×2 cm.[30] A more elegant technique is to apply the k-space filter during data acquisition, which increases S/N.[29] Since signal is only measured from the volume selected by STEAM or PRESS, any combination of FOV and number of phase encoded steps can be chosen to get the desired voxel resolution without phase wrap effects, as long as the FOV is larger than the selected volume. Figure 5 shows NAA, Cho, and Lac CSI images from a patient.

CSI can also be implemented without a STEAM or PRESS volume, using, for example, a 90°–180° spin–echo single or multislice excitation with 2D CSI[30] or even a 3D-CSI volume acquisition.[33] These CSI techniques are useful for collecting spectroscopy data from the outer cortex of the brain. Reference 33 implements data collection during repeated interleaved spiral readout gradients to reduce the total data acquisition time (at a cost of reduced S/N). One can think of collecting time domain spectral data during an oscillating gradient as collecting individual time domain points

TABLE II. Comparison of full-width at half-maximum (FWHM) and signal-to-noise ratio (S/N) between PRESS and STEAM spectra in Fig. 4.

	FWHM	S/N
PRESS water peak	1.45	154 000
STEAM water peak	2.01	66 700
PRESS NAA peak	1.49	69.0
STEAM NAA peak	1.55	38.8

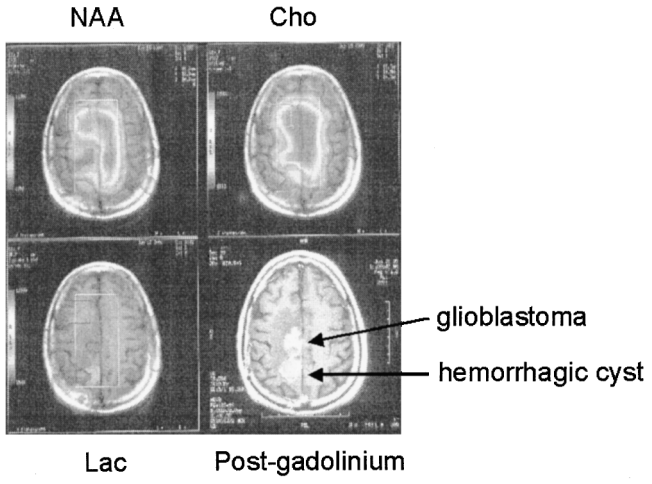

FIG. 5. N-acetyl aspartate (NAA), choline (Cho), and lactate (Lac) chemical shift images superimposed over a T1 weighted image from a patient with a glioblastoma and a hemorrhagic cyst. The lower right image is a post-gadolinium T1-weighted image acquired after the CSI images. The 10 mm CSI slice was acquired with TE=144 ms, TR=1000 ms, 16×16 phase encoding steps, and a 24 cm FOV.

for a repeating series of *k*-space points.[34] Only a few time domain points are collected at each *k*-space point during a single TR, but repeated data acquisitions with different time delays will produce a complete time domain signal for each *k*-space point. These advanced techniques are not currently available in a commercial product.

E. Single voxel vs chemical shift imaging

Proton MRS with CSI acquisition has several advantages over single voxel acquisitions (SVA).

(1) CSI provides better S/N as compared to two or more sequential SVA since the signal from each voxel is averaged for the total data collection time with CSI.
(2) The CSI grid can be shifted after data acquisition (similar to image scrolling), allowing precise positioning of a voxel after data acquisition.
(3) Many more voxels of data are collected in a practical acquisition time.

There are also disadvantages of CSI compared to SVA.

(1) Since with CSI only the whole CSI volume is shimmed rather than each individual voxel as in SVA, the shim for each CSI voxel is not as good as on a SVA voxel in the same location.
(2) The poorer shim causes more problems with lipid contamination although additional techniques, such as outer volume suppression (OVS), can be used to reduce this.[23,29,32] Water suppression will also vary across the CSI volume because of both changes in B1 and magnetic field inhomogeneities.
(3) Because three ''slice'' selective RF pulses are used to select the CSI PRESS or STEAM volume, there are imperfect slice profiles which cause problems for spectra from voxels near the outside of the CSI volume. The resulting alterations in tip angle and phase for different voxel locations will alter *J* coupling effects as a function of location that in turn will make consistent metabolite quantification more difficult. Nonoptimal tip angles at the outer edges of the CSI volume also reduce S/N in the outer voxels.
(4) The minimum CSI data collection time is determined by the required number of phase encode steps and can become long, especially if an unsuppressed water reference set is required. Time cannot be reduced by decreasing the size of *k* space since this increases lipid contamination from the CSI point spread function.[30] The acquisition time can be reduced by 25% with a circularly bounded *k*-space acquisition,[35] a reduced FOV and number of phase encoded steps across the narrow direction of the head[37] (similar to a rectangular field of view in imaging), or with the echo planar imaging (EPI) spectroscopy approach.[33,34]
(5) The metabolite concentrations measured from a spectrum associated with one voxel actually correspond to the integrated metabolite concentrations over the CSI point spread function. This means the measured metabolite concentrations will depend on such factors as voxel location and how quickly metabolite concentrations change spatially throughout the brain. Since the point spread function usually has negative lobes (sinc function) and spectra quantification is done in the absorption mode, metabolite peaks from adjacent voxels will be added in negative phase. This will cause peak shape distortions because adjacent voxels usually have different center frequencies than the voxel of interest.

In summary, consistent, high quality, short TE spectra *in vivo* are best acquired with the SVA technique,[38] but time restraints limit acquiring data from only a few VOIs. CSI is best when more VOIs are required. A long echo time (TE >130 ms) can be used to simplify the spectra and reduce the lipid and macromolecule signal, which will make metabolite quantification reasonably consistent. However, the long TE time reduces the number of quantified metabolites to NAA, Cho, Cr, and lactate.

IV. SIGNAL-TO-NOISE RATIO

Since the MRS time domain signal is complex, two frequency domain signals result from the Fourier transform that are typically labeled ''real'' and ''imaginary.'' These signals are linear combinations of the absorptive and dispersive components of the Lorentzian line shape. In principle proper phase adjustments can make the ''real'' signal purely absorptive and the ''imaginary'' signal purely dispersive.

The signal from a metabolite is the area under its peak. The full-width at half-maximum value (FWHM) of the Lorentzian absorption spectral peak in Hz is defined as, $\mathrm{FWHM}=1/(\pi \mathrm{T2}^*)$, where $1/\mathrm{T2}^*=1/\mathrm{T2}+\gamma\Delta B_0$. For an absorptive Lorentzian peak the area under the peak is equal to $\pi/2*(\mathrm{FWHM})*$ (peak height). For the Lorentzian dispersion component, the peak width is much broader and the area under the peak integrates to zero, so the dispersion peak is not typically used in clinical MRS analysis. A mathematical description of the Lorentzian function can be found below in Sec. XV.

In a well-shimmed spectrum, the peak's height is an easily measured indicator of the signal. Noise in a spectrum can be evaluated by measuring the standard deviation in a region that contains no signal, such as between -1.0 and -2.0 ppm. Therefore, one definition of S/N is the ratio of peak height divided by the rms noise.[27] Under this definition, one manufacturer suggests that the minimum acceptable *in vivo* S/N is five. A second definition of S/N is peak area divided by the rms noise.[39] Both definitions are used in the literature, but careful reading may be required to learn which definition a particular paper uses.

The area of a Lorentzian peak is independent of the shim quality measured by FWHM. Therefore, the second definition is a more absolute measure of S/N and a better parameter for testing hardware performance on a MRS phantom, especially for quality control (QC) and for comparing different hardware. However, *in vivo*, metabolite peaks typically overlap and the precision in determining metabolite peak ar-

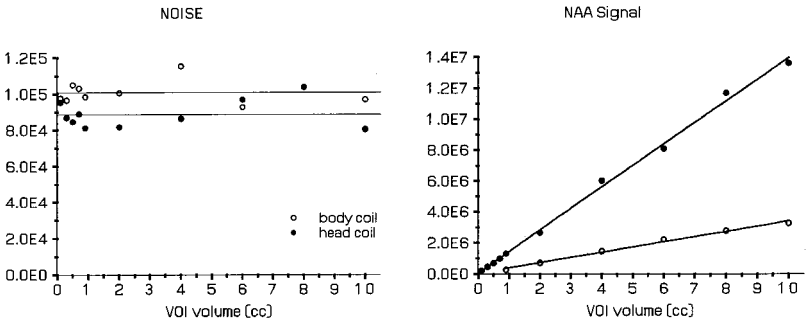

FIG. 6. Effect of changing VOI size on SIGNAL and NOISE. The head coil has more SIGNAL and less NOISE than the body coil.

eas depends as much on the FWHM as on the peak area S/N. Therefore, the first definition of S/N is more pertinent for comparing *in vivo* data and optimizing MRS methodology. Note, however, that metabolite concentrations are calculated from peak areas. In addition, when comparing S/N between two spectra, the comparison will be valid only if identical data acquisition and post-processing were used. These conditions are rarely met when spectra are collected on MR systems from two different vendors. As an example, peak area which is proportional to the amplitude of the first time domain point is usually not affected by post-processing time domain filters, but these filters reduce noise and peak heights. Therefore post-processing filters change peak area S/N differently than peak height S/N.

The magnitude of the noise is independent of the VOI size, but depends on the tissue volume detected by the RF coil, and increases with the square root of the number of signals that were added coherently (n). The magnitude of the signal is directly proportional to the volume of the VOI, proton density, and the number of averages (n). Figure 6 shows the noise and signal in the head and body coils as the VOI size is changed. With respect to the head coil, the noise is 14% higher and the signal 76% lower with the body coil. With averaging, S/N is proportional to $n/\sqrt{n}$, or $\sqrt{n}$.

Averaging is a specific example illustrating the principle that S/N is proportional to the square root of the total signal data acquisition time.[40] Therefore, S/N (peak height) will also depend on the duration of the STEAM or PRESS echo which decays with T2*, assuming that the data acquisition time is $\geqslant 5$T2* in duration. The specific value of T2* will depend on the shim, metabolite T2, and tissue susceptibility. A good single voxel shim in the brain's parietal–occipital lobe will give a linewidth approaching 4 Hz corresponding to a T2*=80 ms. *In vitro* on a spherical phantom, voxel shims below 1 Hz are typical corresponding to a T2*$>$318 ms. Therefore, *in vivo*, an echo data acquisition time of 400 ms ($5\times$T2*) is sufficient, but *in vitro*, data acquisition times $>$1500 ms are required to maximize S/N. When comparing two different MR systems on S/N, one must ensure that both systems are using the same data acquisition time. Also, since in a typical *in vivo* ^{1}H-MRS acquisition TR is $\geqslant$1.5 s allowing a data acquisition time $\geqslant$1 s, S/N will increase from the longer signal duration obtained with better shimming.

Depending on the system software, two of the following three parameters must be set prior to a spectroscopy acquisition: the data acquisition time, the number of complex data points, or the sampling frequency (bandwidth) of the analog-to-digital converter (A/D). Setting two of these automatically calculates the other. Besides having a sufficiently long enough data acquisition time one must also have a high enough sampling frequency to cover the bandwidth of the desired spectrum. Note that this required bandwidth scales linearly with B_0.

V. SHIMMING

The preceding sections have emphasized the importance of magnetic field homogeneity in MR spectroscopy. Improving magnetic field homogeneity increases S/N and narrows peak widths. Thus shimming improves both sensitivity and spectral resolution. Modern clinical MRI systems use automated shimming routines to improve the homogeneity of the magnetic field by monitoring either the time-domain or frequency-domain MRS signal.[41–46] Note that most clinical MR systems only have first-order shims (gradient coil DC offsets) but a few systems have an additional second-order room-temperature shim set. Examples of a good shim and a bad shim in the water and water-suppressed signals are shown in Figs. 7 and 8. Note that the water signal (unsuppressed) is always used for shimming.

The autoshimming algorithm of the MR system and the magnet B_0 homogeneity can be evaluated by using the spherical MRS phantom. The evaluation should meet the following criteria.

Global shim: After applying the manufacturer's clinical auto shim software, usually over a 25 cm FOV, a simple hard RF pulse (typically a 200–500 μs rectangular pulse) plus signal readout without gradients (data acquisition time $>$300 ms) should show a water peak with a FWHM$\leqslant$5 Hz and a full-width at tenth-maximum (FWTM)$\leqslant 5\times$FWHM. This last condition on the FWTM is calculated assuming a Lorentzian line shape and is sensitive to second and higher order magnetic field inhomogeneities. Typical head *in vivo* shims range from 12–20 Hz, FWHM.

Localized shim: Select a single voxel short echo (TE $\leqslant$30 ms) STEAM or PRESS sequence and place a $2\times 2\times 2$ cm^3 voxel at approximately the center of the phantom. Acquire an unsuppressed water spectrum before and after a manual or localized auto shim. Ideally, there should be little or no change in peak width between the two acquisitions and the FWHM should be $<$1 Hz, or a T2*$>$318 ms. The data acquisition time must be greater than $5\times$T2* and the phan-

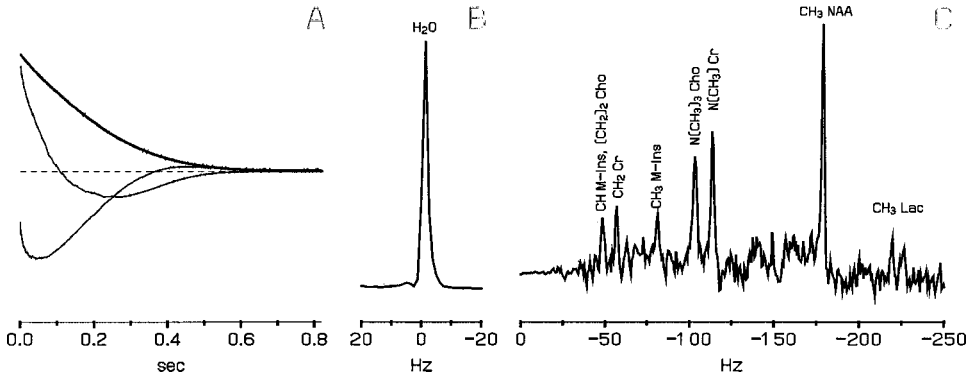

FIG. 7. Example of a good shim. Panel (A) contains the two received channels (light lines) and the magnitude of the water signal in the time domain. Panel (B) contains the absorption spectrum from the water with a FWHM of 1.9 Hz. Panel (C) shows the absorption spectrum with water suppression.

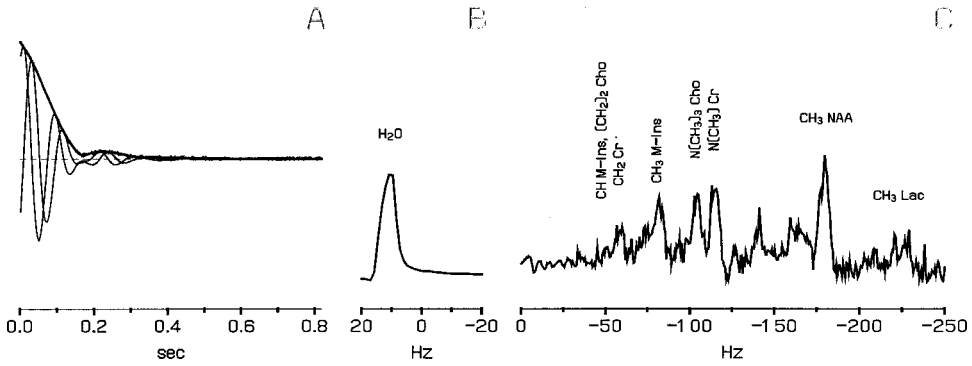

FIG. 8. Example of a bad shim. Panel (A) contains the two received channels (light lines) and the magnitude of the water signal in the time domain. Panel (B) contains the absorption spectrum from the water with a FWHM of 5.6 Hz. Panel (C) shows the absorption spectrum with water suppression. The scaling for the three panels is the same as in Fig. 7.

tom water T2>318 ms. Minimal post-processing of the time domain signal should be used (only zero filling, Fourier transform, and spectral phasing—see Sec. XII). Ideally, the final result should be a Lorentzian peak with no distortions, but in practice, the peak will have some asymmetry due to eddy currents. Note that if apodization was used in post-processing, the apodization line broadening factor will have to be subtracted from the linewidth to get the original linewidth (see apodization filter).

VI. EDDY CURRENTS

Eddy currents are induced in the magnet structure by field gradient pulses. These eddy currents create additional magnetic fields that add to the static field (B_0). Eddy currents can be classified into two categories: one is a zero order eddy current or time-varying B_0 offset which could be compensated with a B_0 coil; the other is a time-varying first or higher order gradient.[47] Zero-order eddy currents will cause a frequency-dependent phase shift during signal readout but no decrease in S/N from spin dephasing within the VOI. First-order eddy currents will dephase the spins within the VOI, decreasing S/N. Both types of eddy currents plus magnetic field inhomogeneities will distort peak shapes, making spectral quantification more difficult, especially when peak fitting to modeled line shapes. The distortion from eddy currents can be corrected by either dividing the ^{1}H spectra time domain signal by the unsuppressed water time domain signal, dubbed *QUA*ntification by converting to the *L*orentz*I*an *TY*pe (QUALITY) deconvolution,[48] or by doing a point by point phase correction of the time domain signal, again using the unsuppressed water signal as a reference often referred to as an Eddy Current Correction (ECC).[49,50] Note that QUALITY will correct peak distortion caused by zero- and first-order eddy currents and B_0 inhomogeneities, while ECC only corrects peak distortion for zero-order eddy currents.

Two hardware approaches can be used to correct for zero-order eddy currents. One is the B_0 compensation coil which would be part of the eddy current compensation hardware. This coil adds or subtracts a uniform field to the main field to keep it at a constant frequency. A second approach is to vary the frequency of the MR system's frequency synthesizer during the signal readout to correct the detected signal frequency for the zero-order eddy currents. This approach requires that a frequency-offset table is generated as part of the eddy current compensation calibration. Eddy current distortion from water spectra (ΔB_0 in Hz)[50] on a magnet without shielded gradient coils and a magnet with shielded gradient coils are illustrated in Fig. 9.

Finally, for short TE spectroscopy the importance of having hardware with low levels of eddy currents cannot be overstated both from our own experience and that of others.[25] Short TE ^{1}H sequences require high amplitude/high slew rate gradients for adequate spoiling in the short durations between and after the selective RF pulses which leads to higher generation of eddy currents. For this reason, we have found that tuning the gradient compensation in a STEAM TE=6 ms sequence can be time consuming and more complex than a STEAM TE=20 ms sequence in which the gradient timing is more relaxed. For the same reason, short TE (~20 to 30 ms) ^{1}H spectroscopy sequences are a good QC tool for checking system eddy currents, even if one does not use the sequence *in vivo*.

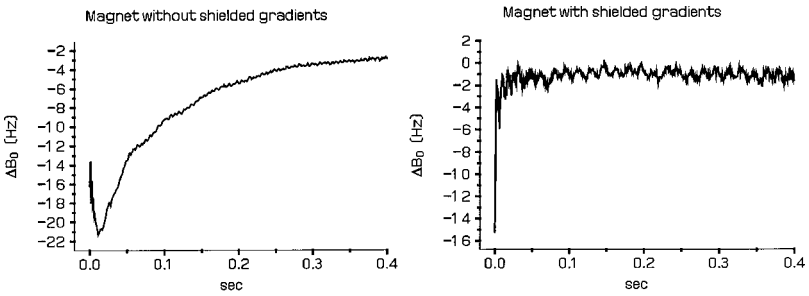

FIG. 9. Eddy current distortions (ΔB_0 in Hz) on a magnet without shielded gradients and on a magnet with shielded gradients. High quality spectra cannot be obtained without shielded gradients, especially at short TE times.

VII. PHASE CYCLING

Physical differences between the two channels of an analog quadrature receiver can introduce artifacts into a magnetic resonance image or magnetic resonance spectrum. There will be ghosting of the peaks mirrored about zero frequency if the phase difference between the two channels is not 90° or the amplifier gains of the two channels are not equal. This is often called a quadrature ghost. If the DC offsets of the two channels are not equal to zero, there will be a spike at zero frequency. *CYCL*ically *O*rdered *P*hase *S*equences (CYCLOPS) can be used to correct for these artifacts.[51] CYCLOPS involves rotating the transmitter phase by 0°, 90°, 180°, and 270°, then adding and subtracting the two receiver channels. CYCLOPS is usually implemented on NMR spectrometers, but not on whole body MR scanners because image acquisitions almost never use four acquisitions. MR scanners do feature a reduced implementation of CYCLOPS, called phase cycling that toggles the transmitter phase between 0° and 180°. The signal obtained with the transmitter phase at 180° is subtracted from the signal obtained with the transmitter phase at 0°. This adds the signal and subtracts the DC offsets. Phase cycling corrects for the DC artifact but does not correct for the quadrature ghost. Another purpose for phase cycling is the compensation for imperfect 180 degree flip angles in multiecho MRI acquisitions.

Modern digital receivers use only one amplifier plus A/D and are no longer plagued with unequal DC offsets, unequal gains, or non 90° quadrature, but phase cycling can still be useful. Multiple data acquisitions are used in single voxel spectroscopy, and CYCLOPS[52] or even more complex phase cycling schemes (Table III) can be used.[53] References 22, 52, and 53 demonstrate that phase cycling can inhibit unwanted transverse magnetization and unwanted echo signals (despite gradient spoiling) from corrupting the spectra. Therefore phase cycling should be used with *in vivo* ^{1}H spectroscopy, when possible. Single voxel acquisitions, which normally use 16 or more data averaging, allow 8 cycle phase cycling as shown in Table III. However, CSI acquisitions rarely have enough data averaging per phase encode step to allow full phase cycling, but even if only two data acquisitions are used at each *k* space point, it is important to phase cycle the third selective RF pulse 0 and 180 degrees to reduce the echo contamination from the third RF pulse FID. RF pulse FIDs arise from nonideal slice profiles and imperfect RF pulse flip angles. In our experience and others[22] the third RF pulse FID is one of the main sources of unwanted transverse coherences because of the limited gradient spoiling available after this last RF pulse.

TABLE III. A possible phase-cycling scheme for a three RF pulse sequence, such as PRESS (see Fig. 2). Note that the total number of signal averages must be a multiple of 8.

Signal excitation	RF pulse phase		
	90°	180°	180°
1	0°	0°	0°
2	180°	0°	0°
3	0°	180°	0°
4	180°	180°	0°
5	0°	0°	180°
6	180°	0°	180°
7	0°	180°	180°
8	180°	180°	180°

VIII. THE PROBLEM WITH WATER

The concentration of pure water is 55.6 M or 111 M for ^{1}H. The water concentration in the brain, calculated from an average MR visible brain water content of 70%, is 36 M.[54] *In vivo* ^{1}H spectroscopy requires water suppression because the 36 M water signal overpowers the 1–10 mM signal of the metabolites. Water suppression is normally accomplished with one or more narrow band (60 Hz) radio frequency CHemical-Shift Selected (CHESS) pulses[20] followed by spoiling gradients at the beginning of the STEAM or PRESS acquisition. This is similar to frequency selective fat RF saturation in imaging. The quality or degree of water suppression depends on the *in vivo* shim, the stability and linearity of the RF amplifier at low power output ($<$0.3 W), the severity of eddy currents, and the number and implementation of the CHESS pulses. For maximal water suppression, the transmitter voltage (flip angle) of the CHESS pulses(s) must be adjusted for each exam. Even though water suppression is optimized for the voxel or volume (CSI) of interest, the water is suppressed globally and will reduce out of volume water contamination.

If only 1 or 2 CHESS pulses are used, the remnant water must be fit and subtracted from the spectrum before peak quantification. The other alternative is to use a very efficient water suppression technique such as *VA*riable *P*ulse power and *O*ptimized *R*elaxation delays (VAPOR)[21,23,55] which reduces the water peak to well below the metabolite peaks.

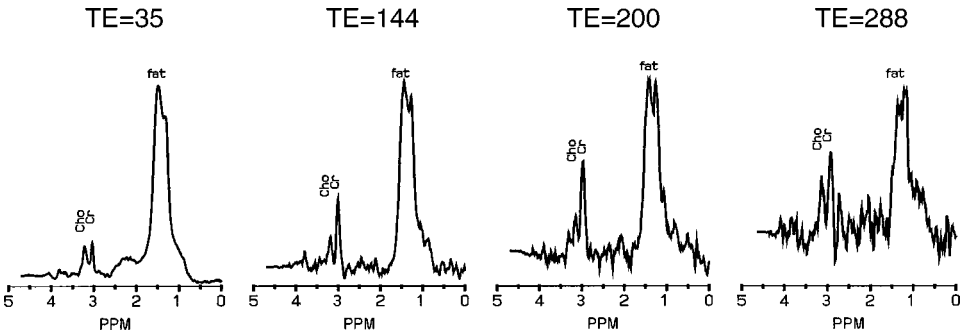

FIG. 10. Reduction of lipid signals as TE is increased. The scans were from a 27 cm^3 volume in the rectus femoris with a PRESS sequence and TR = 1500 ms. As the TE is increased, the fat peak decreases from 16.9 to 0.9. Note that the Cr and Cho signals are also diminished. In general a single voxel acquisition inside the brain with a reasonable shim and gradient spoiling will have the fat signal equal to the metabolite signal at TE = 35 ms and therefore a fat signal buried in the noise at TE = 288 ms.

This technique is also insensitive to CHESS pulse RF power adjustments. Water suppression can also be added during the TM period of a STEAM acquisition.[21] Normally, an unsuppressed water spectrum is acquired by turning off the water suppression RF pulse(s). This signal can then be used for an ECC or QUALITY correction as well as a reference for absolute metabolite quantification.[54,56–64] In order for ECC/QUALITY to work correctly, only the RF pulses are disabled. Making the CHESS crusher gradients constant with and without water suppression will keep the eddy currents consistent.

IX. THE PROBLEM WITH LIPIDS

Another problem associated with *in vivo* proton MR spectra is the ubiquitous presence of lipid peaks. These lipid peaks may obscure other peaks of less abundant metabolites. Lipid contamination usually arises from outside the skull due to nonideal selective slice profiles.[16] Often the spectral contribution of lipids can be reduced by increasing TE, but this strategy also reduces the S/N ratio of all peaks in the spectrum. Other strategies include moving the STEAM or PRESS VOI away from the skull, outer volume saturation bands[16,21,29,32] an inversion pulse[15] similar to Short TI Recovery (STIR) MR imaging, and/or spatial *k*-space data processing before the CSI reconstruction.[36] Note that STIR will also add T1 weighting to the proton metabolites reducing metabolite S/N. The effect of increasing the TE in a PRESS localization scheme can be seen in Fig. 10, where the lipid peak is markedly reduced as the TE is increased from 35 ms to 288 ms. Along with lipids, there are broad macromolecule peaks under the spectrum.[15,16,21] As with lipids, these peaks are reduced with long TE times and/or the lipid STIR technique. However unlike lipids, macromolecule peaks are a natural component of brain tissue present within the selected voxel. Therefore improved slice profiles, outer volume suppression, and improved gradient spoiling, all techniques that reduce lipid contamination, will not reduce macromolecule peaks.

X. SELECTING SPECTROSCOPIC PARAMETERS

Determining the proper parameters for MR spectroscopy will often depend on the type of clinical study. As an example, the following guidelines have been listed for standard brain spectroscopy (cranial tumors).

(1) Secure the head firmly before the study so there will be a minimum voxel displacement. Also, since arm or leg motion will affect the voxel shim, instruct the patient not to fidget. Perform the automated global head shim, center frequency and transmitter power adjustments as normally done with imaging.
(2) Acquire localizer images in three orthogonal planes directly before the MRS scan.
(3) Position and size the voxel of interest. Ensure that the volume of the voxel under investigation is at least 4.5 cm^3. Shim the voxel, either manually or ideally under an automated shim.
(4) Use a TE $\approx$ 144 ms and acquire about 128 scans. The later echo time reduces the signal from macromolecules and from lipid contamination while retaining good S/N. For accurate automated analysis it is recommended that the S/N of Cr should be greater than 5.0. Using TE $\approx$ 288 ms would make the baseline flatter, but scan time should be doubled or voxel size increased by 35% to get spectra with the same S/N as at TE $\approx$ 144 ms.
(5) The use of short TE values ($\leqslant$35 ms) is not recommended because some tumors contain lipids that can cause inaccurate baseline phase correction. For other pathologies, a short TE will provide more information (e.g., myo-inositol), but metabolite quantification will be more difficult because there are more metabolites, lipids, and macromolecule peaks.
(6) Repeat this acquisition for a voxel on the contralateral side to obtain a control spectrum.

XI. PRESCAN ADJUSTMENTS

Before the spectral data are acquired, the MR system will initiate a prescan routine that is often automatic. The prescan will shim the VOI, set the RF transmitter center frequency, set the RF transmitter gain, set the receiver gain, and set the flip angle for the water suppression pulses. On some systems, the VOI will have to be shimmed manually or semiautomatically. If second order or higher resistive shims are available, optimum shim results are obtained by using the higher order shims plus linear shims in a global shim before collecting the localizer images, followed by a localized voxel shim using the linear shims only. The data acquisition without water suppression is acquired by setting the water-suppression pulses to zero flip angle, and should be obtained just before

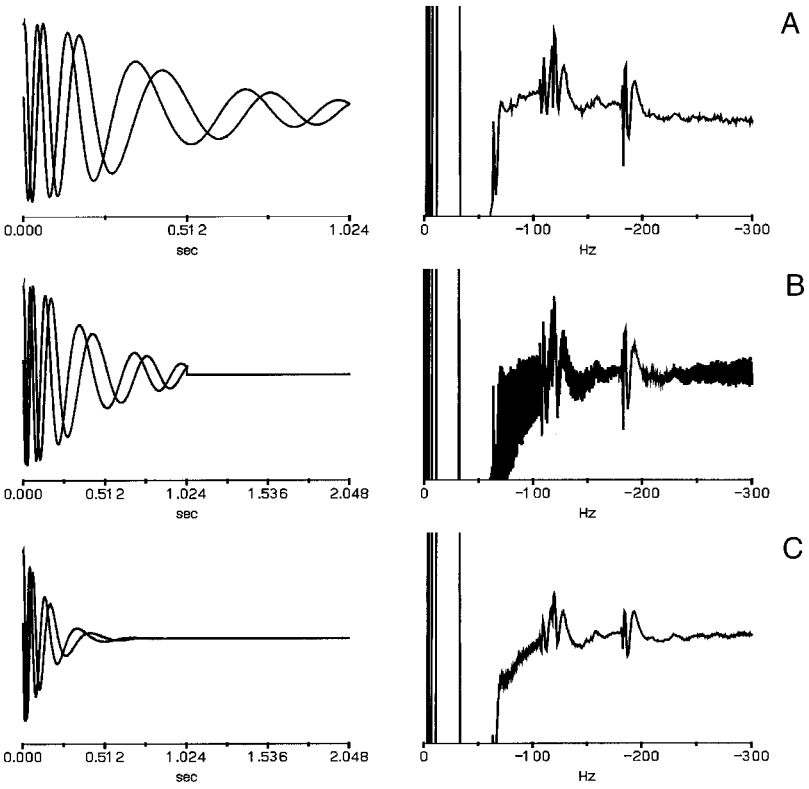

FIG. 11. Post-processing examples of a PRESS (TE $=135$,TR$=3000$) FID from a phantom of pure water and 45 mM methyl protons of NAA, Cr, and Cho. The left panels depict the time-domain signal and the right panels show the absorption spectrum (signal intensity versus frequency) for the same signal. The water frequency was set to zero. The frequency spectrum shows both eddy current distortions and distortions from ''sinc ringing'' because the time domain signal had not decayed to zero by the end of the signal readout. Panel (B) shows the same signals after zero filling the original 1024 data points to 2048 data points. The absorption spectrum displays the higher frequency information that is contained in the first 1024 data points. Panel (C) shows the same data after an apodization filter. This has removed the sinc ringing artifact but at the cost of decreased spectral resolution in the absorption spectrum. The eddy current artifact is still present.

or just after the water-suppressed acquisition. Since water has a much higher concentration, 16 to 32 excitations usually provide sufficient S/N. The water data is used for ECC or QUALITY eddy current correction and sometimes it is used as a reference value for absolute metabolite quantification.

XII. POST-PROCESSING

There are many post-processing techniques used in proton MRS.[54,56–68,71,72] The vendors of clinical MR systems usually provide post-processing software that provides a good starting point and works well, especially for spectra with long TE's. The individual steps embedded in these software packages are described below. In general, these packages fit model peaks to the observed spectrum in the frequency domain with the vendor supplying suggested starting peak templates. However, all post-processing packages will require user tweaking for each different acquisition technique. Some packages also require that the user first acquire *in vitro* data on a set of metabolites to be used for *a priori* knowledge. The *a priori* knowledge can either be measured experimentally or simulated. This will also have to be repeated for each acquisition technique. Typically as much or more time is required to analyze spectra as is expended in developing a MRS protocol and acquiring the MRS data.

Although raw and fitted spectra are displayed in the frequency domain, fitting can be done in either the time or frequency domain. The time domain fit is inherently simpler and slightly more flexible, but the frequency domain fit will give exactly the same final result, provided that all the limitations of the discrete FT are taken into account.[69–71,82] We will discuss some typical techniques and provide illustrations for each step. Several references[27,39,73] provide a general introduction to post-processing.

The signal received in proton MRS, whether it is a free induction decay (FID) or the last half of an echo (i.e., STEAM, PRESS), can be described mathematically as either a damped complex exponential (one component) or a sum of damped complex exponentials (multiple components). The conventional display of an FID signal received in quadrature is as plots of ''real'' signal versus time and ''imaginary'' signal versus time. The conventional display of the FID in the frequency domain is as a correctly phased absorption (real) spectrum although sometimes the dispersive (imaginary) and absolute spectra are displayed as well. However, metabolite concentrations are represented by the absorption spectrum.

We start with a 1024 point water FID acquired with a PRESS sequence (TE$=135$ ms, TR$=3000$ ms, dwell $=1$ ms) on a magnet without self-shielded gradient coils. The phantom consists of a 2 liter round bottom flask containing pure water with 45 mM in methyl protons of NAA, Cr, and Cho. Figure 11(A) shows the signal in the two received channels of the 1024 point FID and the corresponding absorption spectrum with 1024 points (scaled to show the NAA, Cr, and Cho signals). This figure demonstrates eddy current artifacts and the additional ''sinc ringing'' artifact. This latter artifact is equivalent to the Gibb's ringing artifact seen in imaging and has the same source. The time domain data has not reached zero value at the end of the readout period (truncation), which means the time domain data has been multiplied by a box function, which is equivalent to a

sinc convolution in the frequency domain. This effect is also referred to as leakage.[39]

A. Zero filling

Zero filling in the time domain is equivalent to a sinc convolution (interpolation) in the frequency domain. This interpolation improves the visual display of the data in the frequency domain, although no additional information is added. This is identical to image interpolation in MRI. For example, an N point FID has N real and N imaginary, or $2N$ points sampled at Δt intervals. After Fourier transformation, there are N real and N imaginary points with frequency spacing equal to $1/(N\Delta t)$. The spectral width (SW) of the spectrum is $1/\Delta t$ with the abscissa going from SW/2 to $-$SW/2. Zeros can be added to the end of the FID to decrease the frequency spacing over the same bandwidth. Figure 11(B) illustrates zero filling the 1024 point FID to 2048 points in the time domain and the resultant absorption spectrum, which increases the display of the higher frequencies that are contained in the original 1024 data set.

B. Apodization filter

The signal in a free induction decay contains the signal from the metabolites being studied and the noise in the detector channels. A line broadening filter decreases the received signal at the end of the sampling window, which increases the signal-to-noise ratio in a spectrum (peak area definition of S/N) but increases the linewidth of the peak in the frequency domain. This filter multiplies the time domain FID by the filter before transforming to the frequency domain. This weighing of the time domain data is known as apodization. A line broadening filter can also ensure that the FID is not truncated to eliminate sinc ringing (leakage). An exponential filter has the following form:

$$E(t)=\exp(-\pi LBt), \tag{5}$$

where LB is the FWHM of the filter. The time constant of the filter is $\mathrm{TC}=1/(\pi LB)$. A matched filter has a time constant equal to the time constant of the FID and will increase the FWHM by a factor of 2. This filter reflects an optimum balance between the line broadening and noise reduction. To ensure that the tail of the filtered FID is zero, the LB should be $\geqslant 5/(\pi N\Delta t)$ where N is the number points in the FID and Δt is the dwell time in sec. Figure 11(C) shows the result of a 1.5 Hz line broadening filter in the time and frequency domain. Reference 64 describes other filters. Since peak height is equal to the ''integral of the FID'' (sum of time domain magnitude points), expanding the readout time ($N\Delta t$) will increase the peak height (assuming there is still some signal left) while a line broadening filter will decrease the peak height.

C. Eddy current correction

Figure 12 illustrates the ECC method of correcting the spectrum for eddy current caused distortions. Panel (A) shows the water unsuppressed signal (water suppression RF pulses turned off) while panel (B) shows the water suppressed signal (water suppression RF pulses turned on) for a PRESS acquisition. Both (A) and (B) illustrate the artifacts caused by eddy currents. Panel (C) was calculated by subtracting the phase of the unsuppressed water from the phase of the suppressed water at each time domain point. This has dramatically reduced the effects of eddy currents and has almost correctly phased the spectrum as well. Note that QUALITY or a combined QUALITY/ECC technique can also be used for eddy current correction.[48,74]

D. Water suppression filter

Often the water suppression used with proton spectroscopy does not completely eliminate the water signal. Postprocessing with a convolution difference filter can be used to eliminate any residual water signal.[27,39,75] This filter applies a low-pass filter to the FID, then subtracts the filtered signal from the original data in the time domain. The low frequency component is obtained by convolution with either a sine-bell window function or a Gaussian window function.[75] Figure 13 shows processing with a convolution difference filter. The input to the convolution difference filter is the two time domain channels of the FID. The low-pass component (calculated with a 50 Hz sine-bell filter) contains the residual water signal and the high-pass component contains the signals from the metabolites. Note that this method assumes the water resonance is centered near the zero frequency. The absorption spectrum in Fig. 13 shows well-defined NAA, Cr, and Cho peaks with no water peak as in Fig. 12. Another technique to eliminate or reduce water fits a set of peaks using a linear least squares algorithm to the water peak and subtracts this from the FID.[65] Hoch and Stern state that both techniques work equally well.[39]

E. Fourier transform

Any periodic function can be expressed as the sum of sinusoids of different frequencies and amplitudes. The Fourier transform is a method for evaluating the frequencies and amplitudes of these sinusoids. An algorithm for calculating a Fourier transform with a computer was published by Cooley and Tukey and is now known as a fast Fourier transform (FFT).[2] The FFT treats the signal as a periodically repeated function, whether it is or not.[69] When the signal is a free induction decay, there is a sudden jump between the last point (which is usually equal to zero) and the first point (which has the greatest amplitude). This sudden jump in the time domain will produce a DC offset in the frequency domain equal to half the first point of the FID. If the first point of the FID is divided by 2 before transformation, this DC offset will be eliminated.[76] The top curve in Fig. 14 (solid line) is the FFT of a FID with $S(0)=100$ and $\mathrm{T2}^*=10$ ms without dividing the first point by 2, and the DC offset is 50.

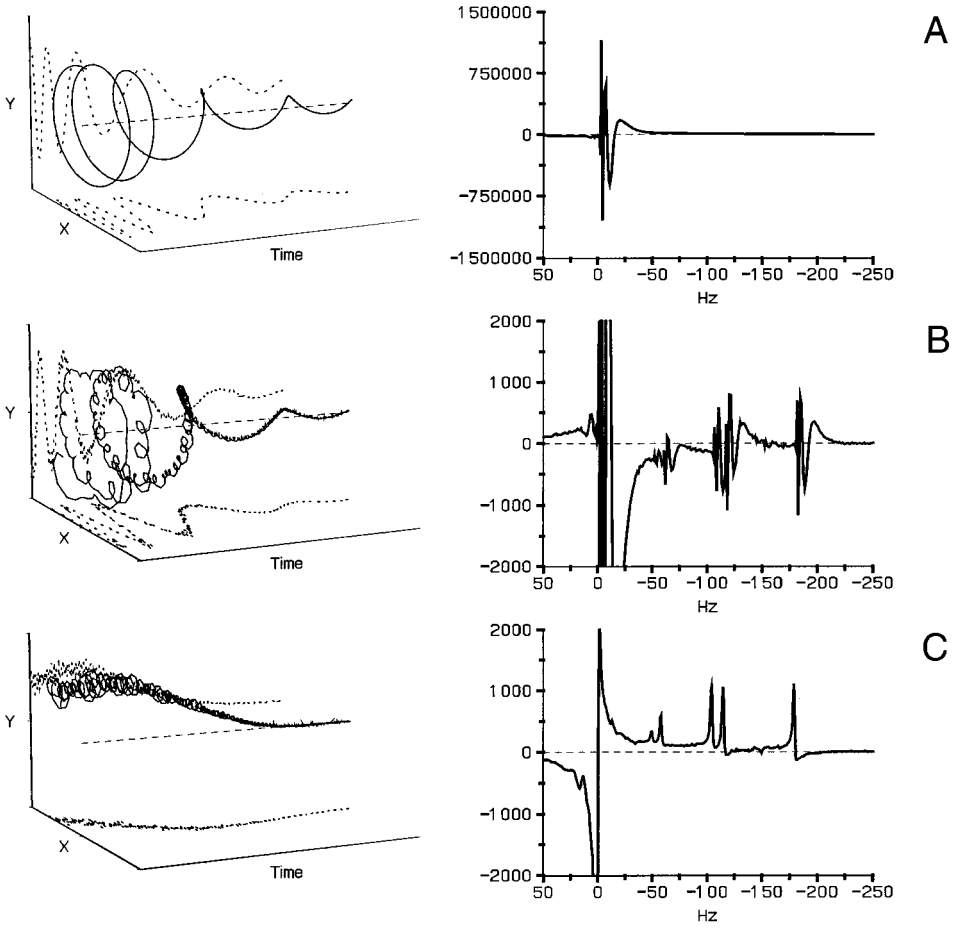

FIG. 12. Post-processing example of eddy current correction (ECC) technique for a PRESS (TE=135,TR =3000) FID from a phantom of pure water and 45 mM methyl protons of NAA, Cr, and Cho. Panel (A) shows the water unsuppressed time domain and absorption signals. Panel (B) shows the water suppressed signals acquired with the water suppression RF pulses switched on. Both (A) and (B) show the same eddy current distortions. Panel (C) was calculated by subtracting the phase of each time domain data point in (A) from the phase of the same time domain data point in (B) (ECC correction). Although ECC automatically gives the correct zero-order phase, some first-order phase correction is still required in panel (C).

The bottom curve in Fig. 14 (dashed line) is the FFT of the FID after dividing the first point by 2, and there is no DC offset.

F. Phasing

Whenever the initial phase of an FID [ϕ in Eq. (11)] is not zero, the real and imaginary channels after Fourier transform will contain mixtures of absorption mode and dispersion mode spectra [Eqs. (14) and (15)]. Phasing a spectrum sorts the real and imaginary channels into absorption mode and dispersion mode spectra:

$$\text{Absorption}(f) = \text{Re}(f)\cos(\theta) + \text{Im}(f)\sin(\theta), \tag{6}$$

and

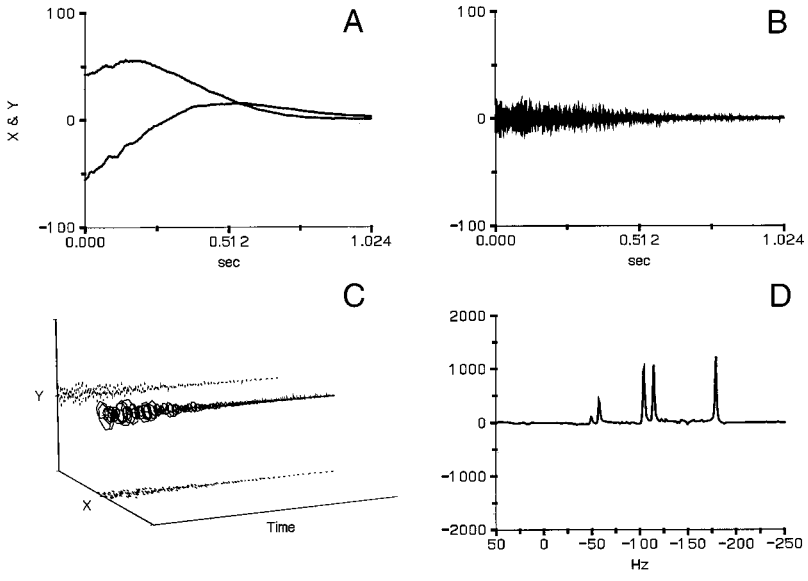

FIG. 13. An illustration of the convolution difference technique for removing the remnant water signal from a ^{1}H spectrum. The starting spectrum is the one from Fig. 12, panel (C). Panel (A) is the time domain output from the low frequency filter. Panels (B) and (C) are the time domain outputs of the high-pass filter and panel (D) is the spectrum from the high-pass filter.

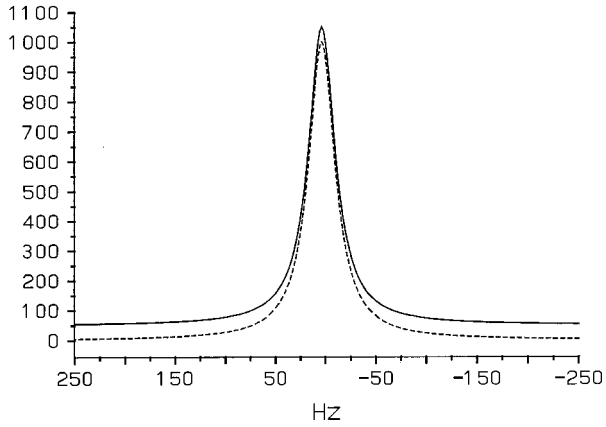

FIG. 14. The DC offset of the signal peak, as seen on the solid line, can be eliminated by setting the first data point of the FID to one-half its measured value before the Fourier transform.

$$\text{Dispersion}(f) = \text{Im}(f)\cos(\theta) - \text{Re}(f)\sin(\theta). \quad (7)$$

Phase (θ) is the sum of the zero-order phase (Z) (constant for all frequencies) and the first-order phase (F) (linear with frequency) and is defined by the following equation:

$$\theta = Z + F\left(\frac{f}{SW}\right). \quad (8)$$

The zero-order phase term corrects for the initial phase of the FID. For a single spin compound, θ in Eqs. (6) and (7) is equal to ϕ in Eq. (11) and can be determined by taking the four-quadrant arctangent of the first data point in the time domain FID.

Delay in the time domain corresponds to a frequency dependent phase shift in the frequency domain. The first-order phase term is necessary whenever the start of the A/D sampling window does not start at the peak of the damped exponential. A DISPA plot is obtained by displaying the real and imaginary data in a "*XY*" plot.[77]

To illustrate phasing, a time domain FID with a dwell time of 1 ms and two components was generated with Eq. (11), then converted to the frequency domain with an FFT. One exponential had $f_0 = 0$ Hz, $S(0) = 100$, and T2* $= 100$ ms. The other exponential had $f_0 = 250$ Hz, $S(0) = 200$, and T2* $= 50$ ms. The peak heights for both peaks will be 10 000. For Fig. 15(A), $Z = 0°$ and there was no time delay. Like FIDs, MR spectra are complex data sets (real, imaginary, or some combination), as illustrated in Fig. 15. The projection in the real plane is the absorption spectrum and the projection in the imaginary plane is the dispersion spectrum. (The DISPA plot, not shown here, is the projection in the real–imaginary plane.) For Fig. 15(B), a FID with the two exponentials was generated with $Z = 45°$ and no time delay. The spectrum in Fig. 15(B) shows the spectrum rotated 45°, producing spectra in the real and imaginary planes that are mixtures of the absorption and dispersion spectra. This spectrum will require a zero order phase of 45°.

For Fig. 15(C), a FID with the two exponentials was generated with $Z = 0°$ and a 1 ms time delay. One terminology for specifying the delay is as dwells, which is the number of

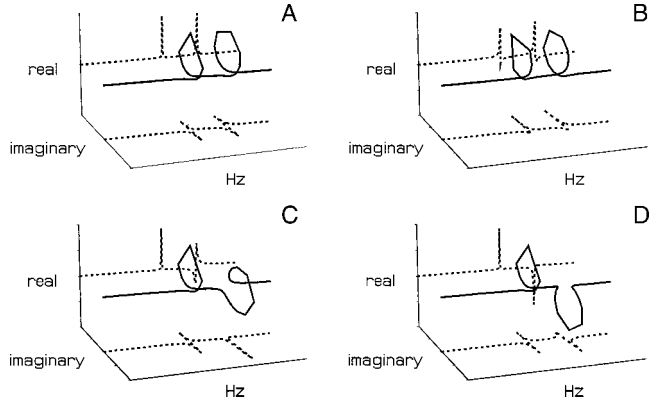

FIG. 15. Complex plots of a spectrum containing two components demonstrating zero- and first-order phasing. In panel (A), both zero- and first-order phases are equal to zero. The projection in the real plane is the absorption spectrum and the projection in the imaginary plane is the dispersion spectrum. In panel (B), the zero-order phase is 45° and the first-order phase is zero. In panel (C), the zero-order phase is zero and the first-order phase is −360°. In panel (D), the zero-order phase is zero and the first-order phase is −720°.

dwell times the FID is delayed. In this case, dwells = 1. A second terminology would refer to this as a left shift = 1. The spectrum in Fig. 15(C) is twisted. The loop at 0 Hz produces an absorption peak in the real plane and the loop at 250 Hz produces an absorption peak in the imaginary plane. This spectrum will require a first order phase of −360°. For Fig. 15(D), a FID with two exponentials was generated with $Z = 0°$ and a time delay of 2 ms, or 2 dwells. The spectrum in Fig. 15(D) is twisted with the loop at 0 Hz producing an absorption peak in the real plane and the 250 Hz loop producing an inverted absorption peak in the real plane. This spectrum will require a first-order phase of −720°.

The zero-order phase (Z) is equal to the phase of the first point in the FID (time domain). The zero-order phase is also equal to the four-quadrant arctangent of the sum of the real points and the sum of the imaginary points in the frequency domain, providing that there were no alterations to the FID before Fourier transformation such as applying saturation pulses when acquiring a FID or shifting the time domain points after a FID is acquired (for first-order phase correction).

When correcting water-suppressed spectra for eddy currents with post-processing such as ECC, the phase of a water FID is subtracted from the phase of a water-suppressed FID. Besides linearizing the phase, this subtraction also applies a zero-order phase to the spectra because the phase offset of the water FID is equal to the phase offset of the water-suppressed FID. If the A/D sample window is placed correctly in a STEAM or PRESS sequence, first-order phasing is not required, and the eddy current corrected spectrum is properly phased.

Software post-processing usually has a left shift tool that allows one or more data points to be deleted from the beginning of the complex FID. This is equivalent to changing the delay time by 1 A/D sample point and may correct the A/D sample window position if it was positioned early. Some-

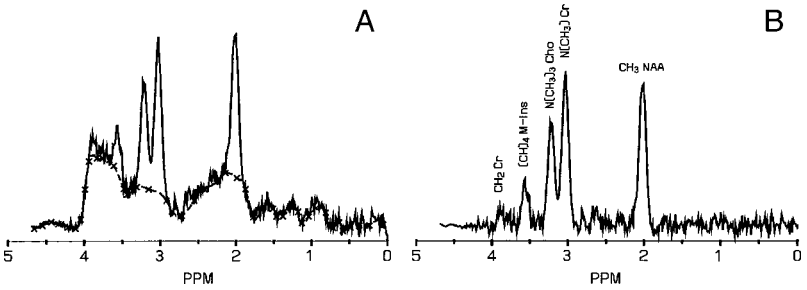

FIG. 16. An *in vivo* PRESS ($TE = 30$ ms) spectrum showing the typical baseline from underlying macromolecule, lipid and J coupled metabolite peaks is shown on the left along with a cubic spline baseline as indicated by the dashed line. The right figure depicts the spectrum resulting from the subtraction of the baseline. This is one of many methods to remove the baseline and not necessarily the optimum technique.

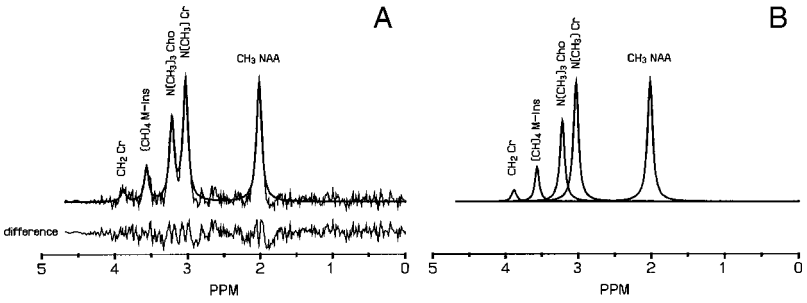

FIG. 17. A demonstration of spectral peak fitting on the baseline corrected *in vivo* spectrum from Fig. 16 using a nonlinear least-squares method. The heavy solid line in panel (A) shows the fitted spectrum and the lower line is the difference between the raw data and the fitted spectrum. Panel (B) shows the individual peaks from which metabolite areas would be calculated.

times, the first points in a FID may be corrupted and these points can be removed with the left shift tool, but first-order phasing will be required to correct for the additional delay time.

G. Baseline correction

The quantification of MR spectra requires evaluating the area under the peaks in the absorption mode spectrum. Distortions of the baseline around these peaks may greatly affect the accuracy of these areas. Methods for defining the baseline of a spectrum include DC offset correction, correction with linear tilts, and cubic or higher order splines. This baseline is subtracted from the spectrum before calculating the areas. As mentioned previously, short TE spectra contain broad lipid and macromolecule peaks that require fitting before metabolite peak areas can be evaluated. Figure 16(A) shows a short TE spectrum from the cerebellum and a cubic spline baseline. Figure 16(B) shows the spectrum after subtracting the baseline. This actually illustrates a poor baseline fit since some of the baseline has been fit to metabolites. Therefore, a better approach to dealing with baseline peaks is to include them in the overall metabolite fitting algorithm, either as a baseline fit[66,78] or to model them as peaks (usually Gaussian).[67]

Discrepancies in metabolite values between investigators often arise from differences in baseline processing.[78] As previously mentioned, long TE spectra usually will not require baseline correction for macromolecules and lipids. In this case a baseline correction may not be required at all as long as there are no other baseline artifacts such as a DC offset or a first-order phase roll.

H. Peak areas

Evaluating the area under a single peak can be done with the traditional running integral, i.e., the running sum of the amplitudes above baseline across the spectrum. This historical technique is illustrated in Fig. 8.6 in de Graaf's book.[79] Another method for measuring the area is to manually select baseline points under a peak, then determine the area between this baseline and the spectral points. However, calculating areas in spectra with multiple, overlapping peaks cannot be evaluated this way.[80] With overlapping peaks, it is necessary to deconvolve the individual peaks to find their areas. Such deconvolution involves fitting a spectrum with Lorentzian, Gaussian, or a Lorentzian–Gaussian mixture of line shapes so that the difference between the observed and fitted spectra is approximately equal to the noise. The fitting process usually utilizes the Levenberg–Marquardt method for nonlinear least squares to determine the f_0, $A(f_0)$, and T2* parameters for each peak. Figure 17(A) illustrates fitting the spectrum from Fig. 16(B) with Lorentzian peaks while Fig. 17(B) shows the individual peaks. The slight misfit shown in the difference spectrum in 17(A) on for example the NAA peak illustrates that eddy currents and/or magnetic field inhomogeneties produce non-Lorentzian line shapes. Although spectral post-processing and fitting has been described as a set of individual steps, a sophisticated post-processing package will often incorporate water subtraction, phasing, and baseline fitting as part of the computer fitting algorithm.[65,67,81,82] The authors discourage manual phasing and baseline fitting since this will lead to poorer results for the final fitted metabolites.

I. Correcting for relaxation and saturation

The measured area under a spectral peak (from a known volume) is directly proportional to the concentration of the metabolite, after normalizing to the number of protons in the metabolite peak. Since spectroscopy sequences do not have $TR = \infty$ and $TE = 0$, the measured area must be corrected for saturation and relaxation effects. Equation (9) is for areas from a PRESS sequence[83] and Eq. (10) is for areas from a STEAM sequence,[57]

$$\text{area}_{\text{corrected}} = \frac{\text{area}_{\text{measured}}}{\exp\left(\frac{-\text{TE}}{\text{T2}}\right)\left[1-\exp\left(\frac{-\text{TR}}{\text{T1}}\right)\right]} \tag{9}$$

$$\text{area}_{\text{corrected}} = \frac{\text{area}_{\text{measured}}}{\exp\left(\frac{-\text{TE}}{\text{T2}}\right)\left[1-\exp\left(\frac{-(\text{TR}-\text{TM}-\text{TE}/2)}{\text{T1}}\right)\right]\exp\left(\frac{-\text{TM}}{\text{T1}}\right)}. \tag{10}$$

Since the STEAM echo arises from the longitudinal magnetization stored at the beginning of the TM interval, the additional term in Eq. (10) accounts for the loss of the longitudinal magnetization by T1 decay during the TM interval.

T1 and T2 values can be found in the literature for some metabolites in various tissues at some specific B_0 field strengths.[57,59,60,62,84,85] Most clinical MRS papers do not correct for T1 or T2 effects since typically spectral changes are studied over time, or spectra from a group of normal subjects are compared to spectra from a group of subjects with a pathology. Therefore, a constant correction term for T1 or T2 relaxation will not change the results. However, if metabolite levels are altered in a diseased state or over time, one can never rule out that these changes are due to changes in metabolite T1 or T2 relaxation times rather than actual changes in metabolite levels. Although a few authors have measured metabolite T1 and T2, this is a very time-consuming procedure since spectra have to be acquired at several TR/TE time points.[57,60,61] Since the effects on peak distortions due to *J* coupling change with TE, T2 measurements become difficult for metabolites with *J* coupled spins.[14]

J. Calculating concentrations

Methods have been reported that calculate concentration using an internal water signal,[56,57,58] an internal creatine reference,[59] an external reference,[54,60] the amplitude of a nonselective 90° reference pulse,[61] and the amplitude of a modified water-suppression pulse.[62,63] Barantin has written a well-referenced review of absolute quantification.[64] Note that many other NMR mechanisms will need correction factors to get absolute concentrations (p. 377 in de Graaf[79]). For example signal losses from diffusion and nonideal slice profiles will need correction factors.

XIII. MRS EQUIPMENT QUALITY CONTROL (QC)

The MRS phantom should be measured every 1–4 weeks with all the *in vivo* MRS acquisition techniques. Water and metabolite peak areas, peak FWHMs, and baseline noise should be recorded. The water peak area is from a water-unsuppressed acquisition. Two sequential water unsuppressed spectra should be acquired so that the second can be used for ECC (or QUALITY) processing on the first. Two acquisitions for the water unsuppressed spectra provide more than enough peak area S/N ($S/N > 10\,000$, PRESS, TE $= 135$ ms, $2\times2\times2$ cm^3, TR $= 1500$ ms, 1024 ms readout, 0.9 Hz exponential filtering post-processing). Phantom metabolite peak area S/N will depend on the metabolite concentrations. As an example, a phantom with 100 mM acetate has a $S/N > 100$ for two acquisitions with the same parameters as above while for 10 mM, the expected S/N will be greater than 10. Since *in vivo* studies often reference metabolite peak areas to the internal unsuppressed water peak area, the most relevant QC parameter will be the ratio of metabolite peak area to the unsuppressed water peak area. This ratio should have an approximately 1% variance for acetate (100 mM, two acquisitions or 10 mM, 256 acquisitions). For the phantom with the concentrations listed in the caption of Fig. 1, the expected coefficient of variation ranges from 3% for NAA to 6% for M-Ins for an 8 ml volume, 128 acquisitions, TR/TE 1500/30, PRESS sequence[86] and as low as 1% for NAA, Cr, and Cho, for an 8 ml volume, 256 acquisitions, TR/TE 2000/136, PRESS sequence.[87] Note however, that *in vivo* results have much poorer precision.[88]

An excellent phantom test for hardware stability is to observe the water-suppressed water signal with the RF adjusted to maximum water suppression and (usually) maximum receiver gain. Visually, inspect the remnant water peak signal from acquisition to acquisition. Amplitude fluctuations below 10% are excellent. This is a good hardware test especially for low level RF stability, but since some type of water subtraction is done in ^{1}H spectroscopy post-processing, the final spectral quantification may not be affected by unstable water suppression, as long as a sophisticated water fitting/suppression routine is used in post-processing. If these hardware instabilities also occur during the RF volume selective pulses and rephasing gradients, spectra will be degraded.

The unsuppressed water peak is also useful for looking at overall system stability, especially if the data can be acquired and displayed in real time in the frequency domain. Usually, this is done after performing a localized shim with a STEAM or PRESS sequence. Continuously acquire data and measure changes in peak position and signal amplitude for an hour. The peak position should not change by more than 1 Hz while the peak amplitude typically varies around 1%. Note that the typical manufacturer's specification of <0.1 ppm field drift (6 Hz at 1.5 T) will not affect image quality but will degrade *in vivo* ^{1}H spectra since *in vivo* localized line widths can be $\leqslant 5$ Hz and data collection can require 30 minutes. Field drifts in only one direction are typically caused by the magnet. Oscillating field drifts are probably caused by temperature fluctuations in the passive shielding (if it exists), in the passive shims (if they exist), current drifts in the room temperature shim supplies (if they exist) or, less

likely, drifts in the system frequency synthesizer. Variations in peak amplitude, shape, or phase are most likely caused by gradient instabilities.

Since spectral localization depends on the complex interactions between crafted RF pulses and pulsed gradient fields, it is useful to verify the accuracy of the VOI selected by the MR spectroscopic process. This accuracy can be verified by using a phantom with discrete solutions of metabolites at various locations. Volume-of-interest accuracy should be tested for both single voxel and CSI spectroscopy. Generating an image of the localized VOI, obtained with water suppression inactive, can validate the localization accuracy of a specific clinical study. This image is acquired with standard readout and phase encoding gradients added to the MRS pulse sequence.

Any hardware problems in RF linearity, both phase and amplitude, will cause poorer localization which in turn will increase spectral baseline distortion from out-of-volume contamination. Problems in the gradients, for example, eddy currents, will manifest as increased peak distortion in the non-ECC-corrected spectra, especially in short acquisitions. Therefore, equipment QC for spectroscopy requires close monitoring of on-line signals and the unprocessed data, as well as the final numbers produced by the post-processing software.

XIV. COMMENTS FOR HIGH FIELD SPECTROSCOPY

Systems with B_0 greater than 1.5 T are becoming widespread. The advantages for ^{1}H spectroscopy are linear increases in signal-to-noise and metabolite peak separation with increased B_0. Since J coupling constants do not change with B_0, the multiplet groups will become further separated in frequency while the J coupled multiplets within each group will stay at the same spacing. When displaying spectra with a parts-per-million scale, the J coupled peaks will appear closer as B_0 is increased (see Fig. 1). Additionally, Fig. 1 shows that the effects of J coupling are B_0 dependent.[14,89] Therefore, quantification methods that require metabolite templates need new templates at each field strength.

Although the increase in S/N with higher B_0 fields should allow smaller voxels or faster patient measurement times, other effects counter these gains. The high-field MRI literature shows that T2* decreases with increased field strength. Even at 3 T S/N gains can be nullified by decreases in T2*.[90] Our own experience is that spectral linewidths double going from 1.5 to 4.0 T regardless of voxel size or shimming protocol. This almost nullifies the 2.7-fold gain in spectral dispersion for this particular change in field strength. An additional signal loss mechanism is diffusion. Since the selective gradient strength must increase to keep a constant volume selective chemical shift artifact with increasing B_0, the signal loss from diffusion increases. Diffusion signal loss is also worse with long echo times, although creative pulse sequence design can ameliorate some of the signal loss.[89] As in high field micro-MR imaging, the optimum solution is ultrashort TE combined with higher order shimming.[21] An additional advantage of ultrashort TE spectroscopy is the ability to quantify J coupled metabolites such as glutamate and glutamine. With short TE spectroscopy, macromolecule signals dominate the spectra baseline, which have to be accounted for during spectral quantification or nulled during spectral acquisition with an inversion pulse.[15,67,68] Also, RF power requirements increase dramatically because RF power increases with the square of B_0 and the RF bandwidth.[91] The bandwidth has to increase to reduce the volume selective chemical shift artifact and/or to achieve ultrashort echo times.

A final comment: Signal loss from diffusion has sometimes been mistaken for a decrease in T2 with field strength. Proton metabolite T2's remain relatively constant with B_0 and are long compared to water, typically in the 100–400 ms range.[92]

XV. MATHEMATICS USED IN SPECTROSCOPY

The Lorentzian characteristic of the NMR signal have been mentioned above but a more complete mathematical description is now presented (for references see, for example, chap. 1,[79] or Sec. 2.1.4.[27] The time domain signal of water can be described mathematically as a damped complex exponential,

$$S(t)=S(0)e^{i(-2\pi f_{\mathrm{rot}}t+\phi)-t/T_2^*}, \tag{11}$$

where $S(0)$ is the magnitude of the FID at $t=0$, f_{rot} is the frequency of the rotating frame (Hz), and ϕ is phase offset at $t=0$.

The time domain FID can be transformed to the frequency domain with a Fourier transform. Spectroscopists call this peak a Lorentzian. When the phase offset (ϕ) is zero, the real and imaginary components are absorption mode $[A(f)]$ and dispersion mode $[D(f)]$ spectra

$$A(f)=\frac{1}{\Delta t}\frac{S(0)T_2^*}{1+[2\pi T_2^*(f-f_0)]^2} \tag{12}$$

and

$$D(f)=\frac{1}{\Delta t}\frac{S(0)2\pi(T_2^*)^2(f-f_0)}{1+[2\pi T_2^*(f-f_0)]^2}, \tag{13}$$

where f_0 is the center frequency of the peak. Several relationships between the time domain and the frequency domain with a single spin compound are summarized in Table IV.[93]

General equations for the real and imaginary channels that include phase [θ, Eq. (8)] are given by the following equations:

$$\mathrm{Re}(f)=\cos(\theta)A(f)+\sin(\theta)D(f) \tag{14}$$

and

$$\mathrm{Im}(f)=\cos(\theta)D(f)-\sin(\theta)A(f). \tag{15}$$

TABLE IV. Mathematical relationships of a single spin compound.

	Time domain	Frequency domain
Initial amplitude of FID	$S(0)$	$\frac{A(f_0)\Delta t}{T_2^*}$
''Integral'' of FID $\left(\sum_{i=1}^{n} M_i\right)$	$\frac{S(0)T_2^*}{\Delta t}$	$A(f_0)$
T2*	$\frac{\Delta t \Sigma_{i=1}^{n} M_i}{S(0)}$	$\frac{1}{\pi \mathrm{FWHM}}$
Amplitude of peak	$\sum_{i=1}^{n} M_i$	$A(f_0)$
Peak area $(\int_{-\infty}^{\infty} A(f)df)$	$\frac{S(0)}{2\Delta t}$	$\frac{A(f_0)}{2T_2^*}$
Full-width at half-maximum (FWHM)	$\frac{S(0)}{\pi \Delta t \Sigma_{i=1}^{n} M_i}$	$\frac{1}{\pi T_2^*}$
Full-width at tenth-maximum (FWTM)	$3\times\frac{S(0)}{\pi \Delta t \Sigma_{i=1}^{n} M_i}$	$\frac{3}{\pi T_2^*}$

XVI. RECOMMENDATIONS AND SUGGESTED READING

Expertise in MRS can best be gained from experimenting with the MRS phantom that comes with the clinical MR system. Other experimental NMR systems may be available in Radiology and Biochemistry departments, and understanding the function of these devices will improve the physicist's overall skills in MRS. Due to the complexities of data acquisition in MRS, described above, the physicist without MRS experience must be willing to commit a significant amount of time in order to learn the subtle variances that can influence the MRS measurement.

Fortunately, there is a large body of literature on the subject of MRS. The following is a list of monographs and review articles that the authors have found to be most generally useful. MR Task Group # 9 would especially recommend that de Graaf's book should be consulted as one of the first references for all the referenced topics in this document.

Useful overviews on MRS include the following.

Canet, D., *Nuclear Magnetic Resonance: Concepts and Methods* (Wiley, New York, 1991).

de Graaf, R. A., *In vivo NMR Spectroscopy: Principles and Techniques* (Wiley, New York, 1998).

de Graaf, R. A. and Rothman D. L., ''*In vivo* detection and quantification of scalar coupled 1H NMR resonances,'' Concepts Magn. Reson. **13**, 32–76 (2001).

Frahm, J., Merbolt, K., Hanicke, W., ''Localized proton spectroscopy using stimulated echoes,'' J. Magn. Reson. **72**, 502–508 (1987).

Govindaraju, V., Young, K., Maudsley, A. A., ''Proton NMR chemical shifts and coupling constants for brain metabolites,'' NMR Biomed. **13**, 129–153 (2000).

Hoch, J. C. and Stern, A. S., *NMR Data Processing* (Wiley-Liss, New York, 1996).

Howe, F. A., Maxwell, R. J., Saunders, D. E., and Brown, G. Jr., ''Proton spectroscopy *in vivo*,'' Magn. Reson. Quart. **9**, 31–39 (1993).

Lenkinski, R. E., *MR Spectroscopy*, RSNA Categorical Course in Physics: The Basic Physics of MR Imaging, 1997, pp. 163–174.

Narayana, P. A. and Jackson, E. F., ''Image-guided *in vivo* proton magnetic resonance spectroscopy in human brain,'' Curr. Sci. **61**, 340–350 (1991).

Riddle, W. R. and Lee, H., ''Magnetic resonance: Principles and spectroscopy,'' in *Biomedical Uses of Radiation, Part A: Diagnostic Applications*, edited by W. R. Hendee (VCH Publishers, New York, 1999), pp. 419–480.

Ross, B. and Michaelis, T., ''Clinical applications of magnetic resonance spectroscopy,'' Magn. Reson. Q. **10**, 191–247 (1994).

Salibi, N. and Brown, M. A., *Clinical MR Spectroscopy: First Principles* (Wiley-Liss, New York, 1998).

Sanders, J. A., ''Magnetic resonance spectroscopy,'' in *Functional Brain Imaging*, edited by W. W. Orrison, Jr. (Mosby-Year Book, St. Louis, MO, 1995), Chap. 10.

ACKNOWLEDGMENTS

The authors would like to thank all of our clinical colleagues that have provided input and discussion on the use of MRS. We would also like to thank our graduate students for their work in spectral quantification and spectroscopy sequence development.

[a]Author to whom correspondence should be addressed. Electronic mail: drost@lri.sjhc.london.on.ca

[1] P. G. Webb, N. Sailasuta, S. J. Kohler, T. Raidy, R. A. Moats, and R. E. Hurd, ''Automated single-voxel proton MRS: Technical development and multisite verification,'' Magn. Reson. Med. **31**, 365–373 (1994).

[2] J. W. Cooley and J. W. Tukey, ''An algorithm for the machine calculation of complex Fourier series,'' Math. Comput. **19**, 297–301 (1965).

[3] Y. Ishihara, A. Calderon, H. Watanabe, K. Okamoto, Y. Suzuki, K. Kuroda, and Y. Suzuki, ''A precise and fast temperature mapping using water proton chemical shift,'' Magn. Reson. Med. **34**, 814–823 (1995).

[4] V. Govindaraju, K. Young, and A. A. Maudsley, ''Proton NMR chemical shifts and coupling constants for brain metabolites,'' NMR Biomed. **13**, 129–153 (2000).

[5] N. Salibi and M. A. Brown, *Clinical MR Spectroscopy: First Principles* (Wiley-Liss, New York, 1998).

[6] R. B. Thompson and P. S. Allen, ''Sources of variability in the response of coupled spins to the PRESS sequence and their potential impact on metabolite quantification,'' Magn. Reson. Med. **41**, 1162–1169 (1998).

[7] R. B. Thompson and P. S. Allen, ''Response of metabolites with coupled spins to the STEAM sequence,'' Magn. Reson. Med. **45**, 955–965 (2001).

[8] T. H. Ernst and J. Hennig, ''Coupling effects in volume selective ^{1}H spectroscopy of major brain metabolites,'' Magn. Reson. Med. **21**, 82–96 (1991).

[9] P. S. Allen, R. B. Thompson, and A. H. Wilman, ''Metabolite-specific NMR spectroscopy *in vivo*,'' NMR Biomed. **10**, 435–444 (1997).

[10] J. R. Keltner, L. L. Wald, B. D. Frederick, and P. F. Renshaw, ''*In vivo* detection of GABA in human brain using a localized double-quantum filter technique,'' Magn. Reson. Med. **37**, 366–371 (1997).

[11] H. Lei and J. Peeling, ''Simultaneous spectral editing for gamma-aminobutyric acid and taurine using double quantum coherence transfer,'' J. Magn. Reson. **143**, 95–100 (2000).

[12] B. Ross and T. Michaelis, ''Clinical applications of magnetic resonance spectroscopy,'' Magn. Reson. Q. **10**, 191–247 (1994).

[13] E. R. Danielsen and B. D. Ross, *Magnetic Resonance Spectroscopy Diagnosis of Neurological Diseases* (Marcel Dekker, New York, 1999).

[14] R. A. de Graaf and D. L. Rothman, ''*In vivo* detection and quantification of scalar coupled 1H NMR resonances,'' Concepts Magn. Reson. **13**, 32–76 (2001).

[15] K. L. Behar, D. L. Rothman, D. D. Spencer, and O. A. C. Petroff, "Analysis of macromolecule resonances in ^{1}H NMR spectra of human brain," Magn. Reson. Med. **32**, 294–302 (1994).
[16] U. Seeger, I. Mader, T. Nagele, W. Grodd, O. Lutz, and U. Klose, "Reliable detection of macromolecules in single-volume ^{1}H NMR spectra of the human brain," Magn. Reson. Med. **45**, 948–954 (2001).
[17] J. Frahm, K. Merbolt, and W. Hanicke, "Localized proton spectroscopy using stimulated echoes," J. Magn. Reson. **72**, 502–508 (1987).
[18] P. A. Bottomley, "Spatial localization in NMR spectroscopy *in vivo*," Ann. N.Y. Acad. Sci. **508**, 333–348 (1987).
[19] W. R. Riddle, S. J. Gibbs, and M. R. Wilcott, "Dissecting and implementing STEAM spectroscopy," Magn. Reson. Med. **29**, 378–380 (1993).
[20] J. Frahm, H. Bruhn, M. L. Gyngell, K. D. Merboldt, W. Hänicke, and R. Sauter, "Localized high-resolution proton NMR spectroscopy using stimulated echoes: Initial applications to human brain *in vivo*," Magn. Reson. Med. **9**, 79–93 (1989).
[21] I. Tkác, Z. Starcuk, I.-Y. Choi, and R. Gruetter, "*In vivo* ^{1}H NMR spectroscopy of rat brain at 1 ms echo time," Magn. Reson. Med. **41**, 649–656 (1999).
[22] T. Ernst and L. Chang, "Elimination of artefacts in short echo time 1H MR spectroscopy of the frontal lobe," Magn. Reson. Med. **36**, 462–468 (1996).
[23] C. T. W. Moonen and P. C. M. van Zijl, "Highly effective water suppression for *in vivo* proton NMR spectroscopy," J. Magn. Reson. **88**, 28–41 (1990).
[24] I. Tkác, E. R. Seaquist, and R. Gruetter, "A comparison of several methods for quantification of resolved glucose signals in ^{1}H NMR spectra of the human brain," Proceedings of the International Society for Magnetic Resonance in Medicine, 8th Meeting, Denver, Colorado, 2000, Vol. 3, p. 1938.
[25] I. Tkác, P. Anderson, G. Adriany, H. Merkle, K. Ugurbil, and R. Gruetter, "*In vivo* ^{1}H NMR spectroscopy of the human brain at 7T," Magn. Reson. Med. **46**, 451–456 (2001).
[26] C. T. Moonen, M. von Kienlin, P. C. van Zijl, J. Cohen, J. Gillen, P. Daly, and G. Wolf, "Comparison of single-shot localization methods (STEAM and PRESS) for *in vivo* proton NMR spectroscopy," NMR Biomed. **2**, 201–208 (1989).
[27] D. Canet, *Nuclear Magnetic Resonance: Concepts and Methods* (Wiley, New York, 1991).
[28] D. A. Yablonskiy, J. J. Neil, M. E. Raichle, and J. J. H. Ackerman, "Homonuclear J coupling effects in volume localized NMR spectroscopy: pitfalls and solutions," Magn. Reson. Med. **39**, 169–178 (1998).
[29] J. H. Duyn, J. Gillen, G. Sobering, P. C. M. van Zijl, and C. T. W. Moonen, "Multisection proton MR spectroscopy imaging of the brain," Radiology **188**, 277–282 (1993).
[30] C. T. W. Moonen, G. Sobering, P. C. M. Van Zijl, J. Gillen, M. Von Kienlin, and A. Bizzi, "Proton spectroscopic imaging of human brain," J. Magn. Reson. **98**, 556–575 (1992).
[31] T. R. Brown, B. M. Kincaid, and K. Ugurbil, "NMR chemical shift imaging in three dimensions," Proc. Natl. Acad. Sci. U.S.A. **79**, 3523–3526 (1982).
[32] D. C. Shungu and J. D. Glickson, "Sensitivity and localization enhancement in multinuclear *in vivo* NMR spectroscopy by outer volume presaturation," Magn. Reson. Med. **30**, 661–671 (1993).
[33] E. Adalsteinsson, P. Irarrazabal, S. Tropp, C. Meyer, A. Macovski, and D. M. Spielman, "Volumetric spectroscopic imaging with spiral-based k-space trajectories," Magn. Reson. Med. **39**, 889–898 (1998).
[34] S. Posse, G. Tedeschi, R. Risinger, R. Ogg, and D. Le Bihan, "High speed 1H spectroscopic imaging in human brain by echo planar spatial-spectral encoding," Magn. Reson. Med. **33**, 34–40 (1995).
[35] N. Schuff, F. Ezekiel, A. C. Gamst, D. L. Amend, A. A. Capizzano, A. A. Maudsley, and M. W. Weiner, "Region and tissue differences of metabolites in normally aged brain using multislice 1H magnetic resonance spectroscopic imaging," Magn. Reson. Med. **45**, 899–907 (2001).
[36] C. I. Haupt, N. Schuff, M. W. Weiner, and A. A. Maudsley, "Removal of lipid artifacts in 1H spectroscopic imaging by data extrapolation," Magn. Reson. Med. **35**, 678–687 (1996).
[37] X. Golay, J. Gillen, P. C. van Zijl, and P. B. Barker, "Scan time reduction in proton magnetic resonance spectroscopic imaging of the human brain," Magn. Reson. Med. **47**, 384–387 (2002).
[38] R. Bartha, D. J. Drost, and P. C. Williamson, "Comparing the quantification of single volume and CSI short echo STEAM ^{1}H spectra in the left basal ganglia," Proceedings of the International Society for Magnetic Resonance in Medicine, 4th meeting, New York, NY, 1996, Vol. 2, p. 1182.
[39] J. C. Hoch and A. S. Stern, *NMR Data Processing* (Wiley-Liss, New York, 1996).
[40] E. M. Haacke, R. W. Brown, M. R. Thompson, and R. Venkatesan, *Magnetic Resonance Imaging: Physical Principles & Sequence Design* (Wiley-Liss, New York, 1999), Sec. 15.2.
[41] I. S. Mackenzie, E. M. Robinson, A. N. Wells, and B. Wood, "A simple field map for shimming," Magn. Reson. Med. **5**, 262–268 (1987).
[42] D. M. Doddrell, G. L. Galloway, I. M. Brereton, and W. M. Brooks, "Nodal inhomogeneity mapping by localized excitation—the "NIMBLE" shimming technique for high-resolution *in vivo* NMR spectroscopy," Magn. Reson. Med. **7**, 352–357 (1988).
[43] M. G. Prammer, J. C. Haselgrove, M. Shinnar, and J. S. Leigh, "A new approach to automatic shimming," J. Magn. Reson. **77**, 40–52 (1988).
[44] J. Tropp, K. A. Derby, C. Hawryszko, S. Sugiura, and H. Yamagata, "Automated shimming of B_0 for spectroscopic imaging," J. Magn. Reson. **85**, 244–254 (1989).
[45] P. Webb and A. Macovski, "Rapid, fully automatic, arbitrary-volume *in vivo* shimming," Magn. Reson. Med. **19**, 113–122 (1991).
[46] R. Gruetter, "Automatic localized *in vivo* adjustment of all first- and second-order shim coils," Magn. Reson. Med. **29**, 804–811 (1993).
[47] M. Terpstra, P. M. Andersen, and R. Gruetter, "Localized eddy current compensation using quantitative field mapping," J. Magn. Reson. **131**, 139–143 (1998).
[48] A. A. de Graaf, J. E. van Dijk, and W. M. M. J. Bovee, "QUALITY: quantification improvement by converting lineshapes to the lorentzian type," Magn. Reson. Med. **13**, 343–357 (1990).
[49] U. Klose, "*In vivo* proton spectroscopy in presence of eddy currents," Magn. Reson. Med. **14**, 26–30 (1990).
[50] W. R. Riddle, S. J. Gibbs, and M. R. Willcott, "Removing effects of eddy currents in proton MR spectroscopy," Med. Phys. **19**, 501–510 (1992).
[51] D. I. Hoult and R. E. Richards, "Critical factors in the design of sensitive high resolution nuclear magnetic resonance spectrometers," Proc. R. Soc. London, Ser. A **344**, 311–340 (1975).
[52] P. C. M. Van Zijl, C. T. W. Moonen, J. R. Alger, J. S. Cohen, and S. A. Chesnick, "High field localized proton spectroscopy in small volumes: Greatly improved localization and shimming using shielded strong gradients," Magn. Reson. Med. **10**, 256–265 (1989).
[53] J. Hennig, "The application of phase rotation for localized *in vivo* spectroscopy with short echo times," J. Magn. Reson. **96**, 40–49 (1992).
[54] T. Ernst, R. Kreis, and B. D. Ross, "Absolute quantitation of water and metabolites in the human brain: I: Compartments and water," J. Magn. Reson., Ser. B **102**, 1–8 (1993).
[55] P. J. Hore, "Solvent suppression in Fourier transform nuclear magnetic resonance," J. Magn. Reson. **55**, 283–300 (1983).
[56] P. B. Barker, B. J. Soher, S. J. Blackband, J. C. Chatham, V. P. Mathews, and R. N. Bryan, "Quantitation of proton NMR spectra of the human brain using tissue water as an internal concentration reference," NMR Biomed. **6**, 89–94 (1993).
[57] B. J. Soher, R. E. Hurd, N. Sailasuta, and P. B. Barker, "Quantitation of automated single-voxel proton MRS using cerebral water as an internal reference," Magn. Reson. Med. **36**, 335–339 (1996).
[58] P. Christiansen, O. Henriksen, M. Stubgaard, P. Gideon, and H. B. W. Larsson, "*In vivo* quantification of brain metabolites by 1H-MRS using water as an internal standard," Magn. Reson. Imaging **11**, 107–118 (1993).
[59] J. Frahm, H. Bruhn, M. L. Gyngell, K. D. Merboldt, W. Hänicke, and R. Sauter, "Localized proton NMR spectroscopy in different regions of the human brain *in vivo*. Relaxation times and concentrations of cerebral metabolites," Magn. Reson. Med. **11**, 47–63 (1989).
[60] R. Kreis, T. Ernst, and B. D. Ross, "Absolute quantitation of water and metabolites in the human brain. II. Metabolite concentrations," J. Magn. Reson., Ser. B **102**, 9–19 (1993).
[61] T. Michaelis, K. D. Merboldt, H. Bruhm, W. Hänicke, and J. Frahm, "Absolute concentrations of metabolites in the adult human brain *in vivo*: Quantification of localized proton MR spectra," Radiology **187**, 219–227 (1993).
[62] E. R. Danielsen and O. Henriksen, "Absolute quantitative proton NMR spectroscopy based on the amplitude of the local water suppression pulse: Quantification of brain water and metabolites," NMR Biomed. **7**, 311–318 (1994).
[63] E. R. Danielsen, T. Michaelis, and B. D. Ross, "Three methods of cali-

bration in quantitative proton MR spectroscopy,'' J. Magn. Reson., Ser. B **106**, 287–291 (1995).
[64] L. Barantin and S. Akoka, ''An overview of absolute quantification methods for *in vivo* MRS,'' J. Magn. Reson. Anal. **3**, 21–27 (1997).
[65] H. Barkhuijsen, R. de Beer, W. M. M. J. Bovée, and D. van Ormondt, ''Retrieval of frequencies, amplitudes, damping factors, and phases from time-domain signals using a linear least-squares procedure,'' J. Magn. Reson. **61**, 465–481 (1985).
[66] S. W. Provencher, ''Estimation of metabolite concentrations from localised *in vivo* proton NMR spectra,'' Magn. Reson. Med. **30**, 672–679 (1993).
[67] R. Bartha, D. J. Drost, and P. C. Williamson, ''Factors affecting the quantification of short echo *in vivo* ^{1}H spectra: Prior knowledge, peak elimination, filtering,'' NMR Biomed. **12**, 205–216 (1999).
[68] S. D. Mierisová, A. van den Boogaart, I. Tkác, P. Van Hecke, L. Vanhamme, and T. Liptaj, ''New approach for quantitation of short echo time in *in vivo* 1H NMR spectra of brain using AMARES,'' NMR Biomed. **11**, 32–39 (1998).
[69] R. N. Bracewell, *The Fourier Transform and Its Applications* (McGraw-Hill, New York, 1978), p. 362.
[70] E. O. Brigham, *The Fast Fourier Transform and Its Applications* (Prentice Hall, Englewood Cliffs, NJ, 1988), p. 172.
[71] J. Slotboom, C. Boesch, and R. Kreis, ''Versatile frequency domain fitting using time domain models and prior knowledge,'' Magn. Reson. Med. **39**, 899–911 (1998).
[72] MRUI (Magnetic Resonance User Interface), available at www.mrui.uab.es
[73] P. V. Hecke and S. V. Huffel, ''Special Issue: NMR spectroscopy quantitation,'' NMR Biomed. **14**, 223–283 (2001).
[74] R. Bartha, D. J. Drost, R. S. Menon, and P. C. Williamsom, ''Spectroscopic lineshape correction by QUECC: combined QUALITY deconvolution and ECC correction,'' Magn. Reson. Med. **44**, 641–645 (2000).
[75] D. Marion, M. Ikura, and A. Bax, ''Improved solvent suppression in one- and two-dimensional NMR spectra by convolution of time-domain data,'' J. Magn. Reson. **64**, 425–430 (1989).
[76] G. Otting, H. Widmer, G. Wagner, and K. Wüthrich, ''Origin of t_1 and t_2 ridges in 2D NMR spectra and procedures for suppression,'' J. Magn. Reson. **66**, 187–193 (1986).
[77] A. G. Marshall and F. R. Verdun, *Fourier Transforms in NMR, Optical, and Mass Spectroscopy* (Elsevier Science, Amsterdam, 1990), pp. 11–12, 54–55, 86.
[78] B. J. Soher, K. Young, and A. A. Maudsley, ''Representation of strong baseline contributions in ^{1}H MR spectra,'' Magn. Reson. Med. **45**, 966–972 (2001).
[79] R. A. de Graaf, *In vivo NMR Spectroscopy: Principles and Techniques* (Wiley, New York, 1998).
[80] P. A. Bottomley, ''The trouble with spectroscopy papers,'' Radiology **181**, 344–350 (1991).
[81] D. Spielman, P. Webb, and A. Macovski, ''A statistical framework for *in vivo* spectroscopic imaging,'' J. Magn. Reson. **79**, 66–77 (1988).
[82] J. W. C. van der Veen, R. de Beer, P. R. Luyten, and D. van Ormondt, ''Accurate quantification of *in vivo* ^{31}P NMR signals using the variable projection method and prior knowledge,'' Magn. Reson. Med. **6**, 92–98 (1988).
[83] B. J. Soher, P. C. M. van Zijl, J. H. Duyn, and P. B. Barker, ''Quantitative proton MR spectroscopy imaging of the human brain,'' Magn. Reson. Med. **35**, 356–363 (1996).
[84] R. E. Lenkinski, ''MR spectroscopy,'' *RSNA Categorical Course in Physics: The Basic Physics of MR Imaging* (RSNA, Oak Brook, IL, 1997).
[85] R. Kreis, ''Quantitative localized ^{1}H MR spectroscopy for clinical use,'' Prog. Nucl. Magn. Reson. Spectrosc. **31**, 155–195 (1997).
[86] T. Schirmer and D. P. Auer, ''On the reliability of quantitative clinical magnetic resonance spectroscopy of the human brain,'' NMR Biomed. **13**, 28–36 (2000).
[87] A. Simmons, M. Smail, E. Moore, and S. C. R. Williams, ''Serial precision of metabolite peak area ratios and water referenced metabolite peak areas in proton MR spectroscopy of the human brain,'' Magn. Reson. Imaging **16**, 319–330 (1998).
[88] J. M. Wardlaw, D. F. Signorini, and I. Marshall, ''Re: Serial precision of metabolite peak area ratios and water referenced metabolite peak areas in proton MR spectroscopy of the human brain, Simmons *et al.* 1996, Vol. 16, pages 319–330 1998,'' Magn. Reson. Imaging **17**, 483–487 (1999).
[89] J. Hennig, T. Thiel, and O. Speck, ''Improved sensitivity to overlapping multiplet signals in *in vivo* proton spectroscopy using a multiecho volume selective (CPRESS) experiment,'' Magn. Reson. Med. **37**, 816–820 (1997).
[90] P. B. Barker, D. O. Hearshen, and M. D. Boska, ''Single-voxel proton MRS of the human brain at 1.5 T and 3.0 T,'' Magn. Reson. Med. **45**, 765–769 (2001).
[91] D. I. Hoult, C.-N. Chen, and V. J. Sank, ''The field dependence of NMR imaging: II. Arguments concerning an optimal field strength,'' Magn. Reson. Med. **3**, 730–746 (1986).
[92] S. Michaeli, M. Garwood, XH. Zhu, L. DelaBarre, P. Andersen, G. Adriany, H. Merkle, K. Ugurbil, and W. Chen, ''Proton T(2) relaxation study of water, N-acetylaspartate, and creatine in human brain using Hahn and Carr–Purcell spin echoes at 4 T and 7 T,'' Magn. Reson. Med. **47**, 629–633 (2002).
[93] W. R. Riddle and H. Lee, ''Magnetic Resonance Principles and Spectroscopy,'' in *Biomedical Uses of Radiation, Part A: Diagnostic Applications* (VCH Publishers, New York, 1999), pp. 419–480.